Domain-dependent stability analysis of a reaction-diffusion model on compact circular geometries

Article (Accepted Version)

International Journal of Bifurcation and Chaos

DOMAIN-DEPENDENT STABILITY ANALYSIS OF A REACTION-DIFFUSION MODEL ON COMPACT CIRCULAR GEOMETRIES *

WAKIL SARFARAZ†
School of Mathematical and Physical Sciences, University of Sussex, Pevensey 3
Brighton, BN1 9QH, UK
W.Sarfaraz@sussex.ac.uk‡

ANOTIDA MADZVAMUSE
School of Mathematical and Physical Sciences, University of Sussex, Pevensey 3
Brighton, BN1 9QH, UK
A.Madzvamuse@sussex.ac.uk

Received (to be inserted by publisher)

In this work an *activator-depleted* reaction-diffusion system is investigated on polar coordinates with the aim of exploring the relationship and the corresponding influence of domain size on the types of possible diffusion-driven instabilities. Quantitative relationships are found in the form of necessary conditions on the area of a disk-shape domain with respect to the diffusion and reaction rates for certain types of diffusion-driven instabilities to occur. Robust analytical methods are applied to find explicit expressions for the eigenvalues and eigenfunctions of the diffusion operator on a disk-shape domain with homogenous Neumann boundary conditions in polar coordinates. Spectral methods are applied using chebyshev non-periodic grid for the radial variable and Fourier periodic grid on the angular variable to verify the nodal lines and eigen-surfaces subject to the proposed analytical findings. The full classification of the parameter space in light of the bifurcation analysis is obtained and numerically verified by finding the solutions of the partitioning curves inducing such a classification. Spatio-temporal periodic behaviour is demonstrated in the numerical solutions of the system for a proposed choice of parameters and a rigorous proof of the existence of infinitely many such points in the parameter plane is presented under a restriction on the area of the domain, with a lower bound in terms of reaction-diffusion rates.

Keywords: Reaction-diffusion systems, Dynamical systems, Bifurcation analysis, Stability analysis, Turing diffusion-driven instability, Parameter spaces, Polar coordinates.

1. Introduction

Analysis of reaction-diffusion systems (RDSs) in the context of pattern formation is a widely studied topic [J. D. Murray , 2013; L. E. Keshet , 2005; A. M. Turing , 1952; M. A. J. Chaplain, M. Ganish, I. G. Graham

*
†
‡

, 2001; B. I. Henry, S. L. Wearne , 2007; I. Lengyel, I. R. Epstein , 1992; K. Jin. Lee, W. D. McCormick, J. E. Pearson , 1994; M. Kim, M. Bertram, M. Pollmann, A. V. Oertzen, A. S. Mikhialov, H. H. Rotermund , 2001] in many branches of scientific research. Scholars of mathematical and computational biology [A. Madzvamuse, A. H. W. Chung , 2015, 2014; S. Yan., X. Lian, W. Wang, R. K. Upadhyay , 2014; R. Barreira, C. M. Elliot, A. Madzvamuse , 2011; S. Ghorai, S. Poria , 2016; J. A. Mackenzie, A. Madzvamuse , 2009; P. K. Maini, M. R. Myerscough , 1997; A. Madzvamuse, A. H. W. Chung, C. Venkataraman , 2015] devoted a great deal of attention to fully explore the theory of the dynamics governed by reaction-diffusion systems for a variety of reaction kinetics which include an *activator-depleted* [E. Campillo-Funollet, C. Venkataraman, A. Madzvamuse , 2016; P. Liu, J. Shi, Y. Wang, X. Feng , 2013; A. Madzvamuse, P. K. Maini, A. J. Wathen , 2005, 2003; A. Madzvamuse, P. K. Maini , 2007; A. Madzvamuse, H. S. Ndakwo, R. Barreira , 2016; A. Madzvamuse , 2000], Gierer-Meinhardt [A. Gierer, H. Meinhardt , 1972; B. I. Henry, S. L. Wearne , 2007] and Thomas reaction kinetics [T. Erneux, G. Nicolis , 1993; G. Dimitriu, R. Stefanescu , 2008]. The current work is a natural extension of [W. Sarfaraz, A. Madzvamuse , 2017], in which a full classification of the admissible parameter space associated to the dynamical behavior of *activator-depleted* reaction-diffusion system was explored on stationary rectangular domains. It is a common hypothesis in the theory of biological pattern formation [Y. Fengji, W. Junjie, S. Junping , 2009; P. K. Maini, M. R. Myerscough , 1997], that the emergence of a spatially periodic pattern in the computational simulations of reaction-diffusion systems is connected to the properties of the associated eigenfunctions of the diffusion operator in the corresponding domain. The associated drawback with computational approaches [C. Venkataraman, O. Lakkis, A. Madzvamuse , 2012; A. Madzvamuse , 2006; O. Lakkis, A. Madzvamuse, C. Venkataraman , 2014; A. Bonito, I. Kyza, R. Nochetto , 2013; R. Barreira, C. M. Elliot, A. Madzvamuse , 2011; D. J. Estep, M. G. Lasron, R. D. Williams , 2000; G. Dimitriu, R. Stefanescu , 2008; M. J. Baines , 1994; M. G. Larson, F. Bengzon , 2013; W. Huang, R. D. Russell , 2011] for reaction-diffusion systems is that they lack to provide rigorous insight on the role of the eigenfunctions in the emergence of spatial pattern, thus offering a natural platform to explore the evolution of spatial patterns from a perspective of dynamical systems. Numerous works has contributed to exploring the computational aspect of reaction-diffusion systems [A. Madzvamuse, A. H. W. Chung , 2014; A. Madzvamuse , 2006; V. Thomee, L. Wahalbin , 1975; O. Lakkis, A. Madzvamuse, C. Venkataraman , 2014; A. Madzvamuse, P. K. Maini, A. J. Wathen , 2005, 2003], in which a restricted choice of parameter values are used with a partial reliance on trial and error to obtain the emergence of an evolving pattern either in space or in time. A large variety of such work has also employed the analytical approach [A. M. Turing , 1952; A. Madzvamuse , 2008; P. K. Maini, M. R. Myerscough , 1997; A. Madzvamuse, A. H. W. Chung, C. Venkataraman , 2015; A. Madzvamuse, E. A. Gaffney, P. K. Maini , 2010; A. Madzvamuse, H. S. Ndakwo, R. Barreira , 2016; P. Liu, J. Shi, Y. Wang, X. Feng , 2013], to explore reaction-diffusion systems from a perspective of dynamical systems. The majority of the analytical approaches concluded with certain conditions [A. Madzvamuse , 2008; A. Madzvamuse, A. H. W. Chung, C. Venkataraman , 2015; A. Madzvamuse, E. A. Gaffney, P. K. Maini , 2010; A. Madzvamuse, H. S. Ndakwo, R. Barreira , 2016; P. Liu, J. Shi, Y. Wang, X. Feng , 2013; K. Jin. Lee, W. D. McCormick, J. E. Pearson , 1994] on the characteristics of the stability matrix that theoretically predicts reaction-diffusion systems to exhibit spatial patterns, lacking to extend the analysis to computational consequences of these conditions on the admissible parameter spaces in terms of diffusion-driven instability. Furthermore, from the literature to date [P. Liu, J. Shi, Y. Wang, X. Feng , 2013; I. Lengyel, I. R. Epstein , 1992; Y. Fengji, W. Junjie, S. Junping , 2009; J. Schnakenberg , 1979; D. Iron, J. Wei, M. Winter , 2003; C. Xu, J. Wei , 2012; F. Yi, J. Wei, J. Shi , 2009], it is evident that insufficient attention is given to rigorously explore the influence of reaction-diffusion rates on the dynamical behaviour of such systems in the context of domain size. The motivation of the current work originates from the hypothesis of the spatial dependence of the eigenfunctions of the diffusion operator with the domain size itself and extending this idea to further investigate how this spatial dependence induces an influence on the linearised stability-matrix of a reaction-diffusion system through the properties of the eigenfunctions of the diffusion operator. With an attempt to further contribute to the current knowledge of reaction-diffusion systems, the present paper employs a set of rigorous findings obtained from bifurcation analysis of the *activator-depleted* reaction-diffusion model to explore the corresponding influence induced on the admissible parameter spaces and diffusion-driven instability. Despite the restriction of the current work to a particular type of reaction kinetics namely

activator-depleted, the methodology can however serve as a framework for developing a bifurcation analysis, parameter spaces and computational methods, that could be utilised for general reaction-diffusion systems. The lack of a self-contained complete methodology that combines all the known distinct aspects of exploring this topic creates a credible argument for the importance of this work.

The content of this work is structured such that in Section 2 the model equations for *activator-depleted* reaction-diffusion system are stated in polar coordinates in non-dimensional form with the corresponding initial and boundary conditions. Section 3 consists of a detailed analytical method to explicitly derive eigenfunctions and the corresponding eigenvalues satisfying the boundary conditions prescribed for *activator-depleted* reaction-diffusion system in Section 2. Furthermore, an application of spectral approach on polar coordinates using chebyshev and Fourier grid method is presented [L. N. Trefethen , 2000] to demonstrate and verify the analytical derivation of the eigenfunctions as well as the stability matrix and the corresponding characteristic polynomial for a linearised approximation of the original system. Section 4 presents analytical results on the relationship of domain-size (radius of disk) with different types of bifurcations in the dynamics. Section 5 is devoted to the parameter space classification in light of the bifurcation analysis of the uniform steady-state of the system. A numerical method for computing the partitioning curves for such classification is presented in detail. The shift of parameter spaces as a consequence of changing reaction-diffusion rates is investigated and theorems are proven that rigorously establish the relation of the radius of the disk with the corresponding types of diffusion-driven instabilities. A full classification of the admissible parameter space in terms of stability and types of the uniform steady state of the system is also presented where it is shown that if the radius of a disk-shape domain satisfies certain inequalities in terms of reaction-diffusion rates, then the admissible parameter space allows or forbids certain types of bifurcations in the dynamics of the reaction-diffusion system. Section 6 presents numerical simulations of an *activator-depleted* reaction-diffusion system using the finite element method to verify the proposed classification of parameter spaces and the theoretically predicted behaviour in the dynamics. Due to the curved boundary of the domain a non-standard technique called *distmesh* [O. Persson , 2015; A. Schnepf, D. Leitner , 2009; G. Strang, P. O. Persson , 2004] is used to obtain mesh discretisation for use by the finite element method. Section 7 presents the conclusion and possible extensions of the current work.

2. Model equations

Two chemical species u and v are modelled by the well-known *activator-depleted* reaction-diffusion system, where both species are coupled through nonlinear reaction terms. The system assumes independent diffusion rates for both of the species. The RDS is considered on a two dimensional circular domain denoted by $\Omega \in \mathbb{R}^2$, defined by $\Omega = \{(x, y) \in \mathbb{R}^2 : x^2 + y^2 < \rho^2\}$. This forms a two dimensional disk-shape domain with a circle forming its boundary denoted by $\partial\Omega$, which contains the points given by $\partial\Omega = \{(x, y) \in \mathbb{R}^2 : x^2 + y^2 = \rho^2\}$. The RDS with *activator-depleted* reaction kinetics in its non-dimensional form in polar coordinates has the form

$$\begin{cases} \begin{cases} \frac{\partial u}{\partial t} = & \triangle_p u + \gamma f(u, v), \\ \frac{\partial v}{\partial t} = & d\triangle_p v + \gamma g(u, v), \end{cases} \\ \frac{\partial u}{\partial r}\big|_{r=\rho} = \frac{\partial v}{\partial r}\big|_{r=\rho} = 0, \qquad (r, \theta) \in \partial\Omega, \quad t \geq 0, \\ u(r, \theta, 0) = u_0(r, \theta), \qquad v(r, \theta, 0) = v_0(r, \theta), \qquad (r, \theta) \in \Omega, \quad t = 0, \end{cases} \tag{1}$$

where $\triangle_p$ denotes the Laplace operator in polar coordinates written as

$$\triangle_p u(r, \theta) = \frac{1}{r}\frac{\partial}{\partial r}\Big(r\frac{\partial u}{\partial r}\Big) + \frac{1}{r^2}\frac{\partial^2 u}{\partial \theta^2}. \tag{2}$$

In (1), u and v depend on polar coordinates (r, θ) obtained through the transformation $x = r\cos\theta$ and $y = r\sin\theta$, The functions f and g are defined by $f(u, v) = \alpha - u + u^2 v$ and $g(u, v) = \beta - u^2 v$. In the above, α, β, γ and d are strictly positive real constants. The positive parameter d denotes the non-dimensional ratio of diffusion rates given by $d = \frac{D_v}{D_u}$, where D_v and D_u are the independent diffusion rates of v and u respectively. The non-dimensional parameter γ is known as the scaling parameter which quantifies the strength of the reaction rates. The boundary of Ω under the current study assumes homogeneous Neumann

boundary conditions (also known as zero flux boundary conditions), which means that the chemical species u and v can neither escape nor enter through $\partial\Omega$.

3. Stability analysis of the reaction-diffusion system

Let u_s and v_s denote the uniform steady state solution satisfying system (1) with *activator-depleted* reaction kinetics in the absence of diffusion and these are given by $(u_s, v_s) = (\alpha + \beta, \frac{\beta}{(\alpha+\beta)^2})$ [J. D. Murray , 2013; L. E. Keshet , 2005; W. Sarfaraz, A. Madzvamuse , 2017; A. Madzvamuse, A. H. W. Chung, C. Venkataraman , 2015]. For linear stability analysis, system (1) is perturbed in the neighbourhood of the uniform steady state (u_s, v_s) and the dynamics of the perturbed system are explored i.e. $(u, v) = (\bar{u} + u_s, \bar{v} + v_s)$, where $\bar{u}$ and $\bar{v}$ are assumed small. Taylor expanding system (1) in functions of two variables up to and including the linear terms with the higher order terms discarded leads to the linearised version of system written in matrix form as

$$\frac{\partial}{\partial t}\begin{bmatrix}\bar{u}\\ \bar{v}\end{bmatrix} = \begin{bmatrix}1 & 0\\ 0 & d\end{bmatrix}\begin{bmatrix}\triangle_p\bar{u}\\ \triangle_p\bar{v}\end{bmatrix} + \begin{bmatrix}\frac{\partial f}{\partial u}(u_s, v_s) & \frac{\partial f}{\partial v}(u_s, v_s)\\ \frac{\partial g}{\partial u}(u_s, v_s) & \frac{\partial g}{\partial u}(u_s, v_s)\end{bmatrix}\begin{bmatrix}\bar{u}\\ \bar{v}\end{bmatrix}. \tag{3}$$

What remains is to compute the eigenfunctions of the diffusion operator namely $\triangle_p$, which will require to find the solution to an elliptic 2-dimensional eigenvalue problem on a disk that satisfies homogeneous Neumann boundary conditions prescribed for system (1).

The solution of eigenvalue problems on spherical domains is a well studied area [H. E. William , 1931; N. N. Lebedev , 1965; A. G. Brown, H. J. Weber , 2001], with the majority of research focused on problems with boundary-free manifolds such as circle, torus and/or sphere. Considering the restriction imposed from the boundary conditions prescribed for the current problem, entails that the case requires explicit detailed treatment to rigorously find the eigenfunctions satisfying these boundary conditions. For the sake brevity, we omit a step-by-step demonstration of the process, instead we only submmarise the key parts of this derivation. The eigenvalue problem we want to solve is of the form

$$\begin{cases}\triangle_p w = -\eta^2 w, & \eta \in \mathbb{R},\\ \frac{\partial w}{\partial r}\big|_{r=\rho} = 0, & \rho \in \mathbb{R}_+\backslash\{0\},\end{cases} \tag{4}$$

where $\triangle_p$ is the diffusion operator in polar coordinates defined by (2), on a disk with radius ρ. Application of separation of variables to problem (4) requires a solution of the form $w(r, \theta) = R(r)\Theta(\theta)$, which is substituted into problem (4) to obtain

$$r^2\frac{1}{R}\frac{d^2R}{dr^2} + r\frac{1}{R}\frac{dR}{dr} + \eta^2 r^2 = -\frac{1}{\Theta}\frac{d^2\Theta}{d\theta^2}. \tag{5}$$

Using anzats of the form $\Theta(\theta) = \exp(in\theta)$ and a change of variable $x = \eta r$ is applied to (5). Taking the usual steps of Frobenius method it can be shown that the general solution $R(x)$ satisfying (5) takes the form $R(x) = R^1(x) + R^2(x)$, where $R^1(x)$ and $R^2(x)$ are respectively given by

$$R^1(x) = x^n\sum_{j=0}^{\infty}\frac{(-1)^j C_0 x^{2j}}{4^j \times j! \times (n+j) \times (n+j-1) \times \cdots \times (n+1)} \tag{6}$$

and

$$R^2(x) = x^{-n}\sum_{j=0}^{\infty}\frac{(-1)^j C_0 x^{2j}}{4^j \times j! \times (-n+j) \times (-n+j-1) \times \cdots \times (-n+1)}. \tag{7}$$

Series solutions (6) and (7) are referred to as the Bessel functions of the first kind [J. Spanier, K. B. Oldham , 1987; A. G. Brown, H. J. Weber , 2001]. Noting that $x = \eta r$, the general solution to problem (4) can be written in the form $w(r, \theta) = R(x(r))\Theta(\theta)$. A straightforward application of the chain rule yields $\frac{dR}{dr}\big|_{r=\rho} = \eta\frac{dR}{dx}\big|_{x=\eta\rho}$. Let a_j and b_j denote the coefficients corresponding the jth term in the infinite series for $R^1(x)$ and $R^2(x)$ respectively, defined by

$$a_j = \frac{(-1)^j C_0}{4^j \times j! \times (n+j) \times (n+j-1) \times \cdots \times (n+1)}, \tag{8}$$

$$b_j = \frac{(-1)^j C_0}{4^j \times j! \times (-n+j) \times (-n+j-1) \times \cdots \times (-n+1)}. \tag{9}$$

Then $R(x)$ can be written in the form $R(x) = \sum_{j=0}^{\infty} \left(a_j x^{n+2j} + b_j x^{-n+2j}\right)$. Differentiating $R(x)$ with respect to x and equating it to zero, on substituting $x = \eta\rho$ and using the chain rule we obtain the equation

$$0 = \frac{dR}{dr}\Big|_{r=\rho} = \eta\Big[(\eta\rho)^n \sum_{j=0}^{\infty} a_j(n+2j)(\eta\rho)^{2j-1} + (\eta\rho)^{-n} \sum_{j=0}^{\infty} b_j(-n+2j)(\eta\rho)^{2j-1}\Big], \tag{10}$$

which holds true if and only if both of the summations in (10) are independently zero. Let F_j and S_j denote the jth terms of the first and second summations in (10) respectively, then for (10) to hold true, $F_j + F_{j+1} = 0$ and $S_j + S_{j+1} = 0$ must be true for all $j \in \mathbb{N}$. The full expressions for F_j and F_{j+1} can be written as

$$F_j = \frac{(\eta\rho)^n(-1)^j C_0(n+2j)(\eta\rho)^{2j-1}}{4^j \times j! \times (n+j) \times (n+j-1) \times \cdots \times (n+1)} \tag{11}$$

and

$$F_{j+1} = \frac{(\eta\rho)^n(-1)^{j+1} C_0(n+2j+2)(\eta\rho)^{2j+1}}{4^{j+1} \times (j+1)! \times (n+j+1) \times (n+j) \times \cdots \times (n+1)}. \tag{12}$$

For the first ($j = 0, j = 1$), second ($j = 2, j = 3$) and third ($j = 4, j = 5$) successive pairs, independently equating the sum of the expressions (11) and (12) to zero yields that $\eta_{n,k}^2$ can be written as

$$\eta_{n,k}^2 = \frac{4(2k+1)(n+2k+1)(n+4k)}{\rho^2(n+4k+2)}. \tag{13}$$

This leads us to state the following theorem whose proof is sketched above.

Theorem 1. *Let $w(r,\theta)$ satisfy problem (4) with homogeneous Neumann boundary conditions. Given that the order n of the associated Bessel's function belongs to the set $\mathbb{R}\backslash\frac{1}{2}\mathbb{Z}$, [see Remark 3.1] then for a fixed n there exists an infinite set of eigenfunctions of the diffusion operator $\triangle_p$ as defined in (2), which is given by*

$$w_{n,k} = \left[R_{n,k}^1(r) + R_{n,k}^2(r)\right]\Theta_n(\theta) \tag{14}$$

with the explicit expressions for $R_{n,k}^1(r) = R^1(\eta_{n,k}r)$, $R_{n,k}^2(r) = R^2(\eta_{n,k}r)$ and $\Theta_n(\theta) = \exp(in\theta)$, where for the kth successive pair $\eta_{n,k}$ satisfies (13), when ever $j = 2k$.

Remark 3.1. The restriction on the order of the corresponding Bessel's equation namely $n \in \mathbb{R}\backslash\frac{1}{2}\mathbb{Z}$ in Theorem 1 can be relaxed by employing Bessel's function of the second kind [H. E. William , 1931; A. G. Brown, H. J. Weber , 2001; J. Spanier, K. B. Oldham , 1987] and imposing on it the homogeneous Neumann boundary conditions. Therefore, for the purpose of the current study, the order of the corresponding Bessel's equation is precluded from becoming a full or half integer. Bear in mind that the proposed choice of $n \in \mathbb{R}\backslash\frac{1}{2}\mathbb{Z}$ makes the set of eigenvalues $\eta_{n,k}^2$ a semi discrete infinite set. The spectrum is discrete with respect to positive integers k and continuous (uncountable) with respect to n.

3.1. *Numerical experiments using the spectral method*

Let $R_{n,k}(r)$ denote the expression $R_{n,k}^1(r) + R_{n,k}^2(r)$, then the full set of eigenfunctions to problem (4), can be written as $w(r,\theta) = \sum_{k=0}^{\infty} R_{n,k}(r)\Theta_n(\theta)$. For numerical demonstration of Theorem 1, the spectral method [L. N. Trefethen , 2000] is employed on a unit disk centred at the origin of the x, y coordinates. A spectral mesh in polar coordinates is constructed on a unit disk $\Omega = \{(r,\theta) \in \mathbb{R}^2 : r \in [0,1], \theta \in [0, 2\pi]\}$, where a periodic Fourier grid is applied to the angular axis θ and a non-periodic chebyshev grid is applied to the radial axis r [L. N. Trefethen , 2000]. In order to tackle the singularity at $r = 0$, chebyshev discretisation is applied to the whole of the diameter of Ω, which means that $-1 \leq r \leq 1$ is used instead of $0 \leq r \leq 1$. The interval $[-1, 1]$ is discretised in the form $r_i = \cos(\frac{i\pi}{N})$, for $i = 0, 1, 2, ..., N$, where $N = 2j + 1, j \in \mathbb{N}$,

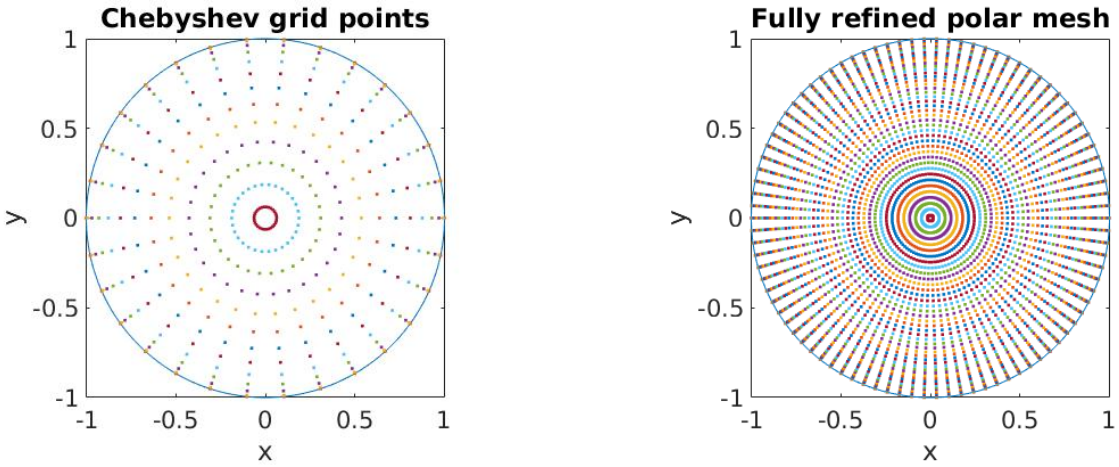

Fig. 1. Mesh generation on polar coordinates obtained from the combination of the chebyshev grid on radial axis and the Fourier periodic grid on angular axis. See main text for mesh parameters

is a positive odd integer. The second coordinate θ is discretised using $\theta_i = \frac{2i\pi}{M}$, for $i = 0, 1, 2, ..., M$, where $M = 2j, j \in \mathbb{N}$, is a positive even integer. Further details on the implementation of the spectral method in polar coordinates can be found in [L. N. Trefethen , 2000]. Fig. 1 shows a refined mesh using $N = 95$ and $M = 90$ with angular step-size of 4°, on which all the simulations for eigenfunctions $w(r, \theta)$ are performed to visualise the corresponding nodal lines and surfaces. Colour encoded plots, corresponding to nine different modes $k = \{1, 2, 3, 5, 6, 7, 9, 12, 15\}$ are simulated on the mesh using a technique presented in [E. Wegert , 2013]. For full details on the implementation of this process the reader is referred to [E. Wegert , 2013]. Fig. 3 shows a colour encoded representation of nine different modes, each of which corresponds to one of the nine nodal line depictions of $w_{n,k}(r, \theta)$ in Fig. 2. Note that in Fig. 2 different modes namely modes 2 and 3 result in the same eigenvalues that correspond to a different orientation of the nodal line depiction for $k = 2$ and $k = 3$. Similarly, one may find that there are a lot of such pairs of positive integers k and $k+1$, that correspond to different orientations of the same nodal line depiction. This occurs, when the multiplicity of an eigenvalue $\eta_{n,k}$ is 2, and in fact there are numerous such pairs of $w_{n,k}(r, \theta)$ and $w_{n,k+1}(r, \theta)$, that correspond to the same $\eta_{n,k}$, but for different orientation of eigenmodes. However applying the colour encoded representation using the (HSV) colour scheme indicates a distinction between the plots corresponding to each integer value for k as shown in Fig. 3.

3.2. *Stability matrix and the characteristic polynomial*

The solution to system (1) using separation of variables, can be written (with bars omitted from $\bar{u}$ and $\bar{v}$) as the product of the eigenfunctions of the diffusion operator $\triangle_p$ and $T(t)$ in the form $u(r, \theta, t) = \sum_{k=0}^{\infty} U_{n,k} \exp(\sigma_{n,k} t) R_{n,k}(r) \Theta_n(\theta)$, and $v(r, \theta, t) = \sum_{k=0}^{\infty} V_{n,k} \exp(\sigma_{n,k} t) R_{n,k}(r) \Theta_n(\theta)$, where $U_{n,k}$ and $V_{n,k}$ are the coefficients associated with the mode of the eigenfunctions in the infinite expansion. Substituting this form of solution in (3) and the steady state values in terms of the parameters α and β for (u_s, v_s), one obtains the fully linearised form of (1) as a system of two algebraic equations. By defining $\mathcal{T}(\alpha, \beta)$ and $\mathcal{D}(\alpha, \beta)$ to denote, respectively, the trace and determinant of the stability matrix of the linearised system, it can be shown straightforwardly that the dispersion relation is a quadratic polynomial of the form

$$\sigma^2 - \mathcal{T}(\alpha, \beta)\sigma + \mathcal{D}(\alpha, \beta) = 0, \tag{15}$$

where

$$\begin{cases} \mathcal{T}(\alpha, \beta) = & \gamma \frac{\beta - \alpha - (\beta + \alpha)^3}{\beta + \alpha} - (d+1)\eta_{n,k}^2, \\ \mathcal{D}(\alpha, \beta) = & \big(\gamma \frac{\beta - \alpha}{\beta + \alpha} - \eta_{n,k}^2\big)\big(- \gamma(\beta + \alpha)^2 - (d+1)\eta_{n,k}^2\big) + 2\gamma^2 \beta(\beta + \alpha). \end{cases} \tag{16}$$

The roots of equation (15) in terms of $\mathcal{T}$ and $\mathcal{D}$ are $\sigma_{1,2} = \frac{\mathcal{T} \pm \sqrt{\mathcal{T}^2 - 4\mathcal{D}}}{2}$. Stability of the uniform steady state (u_s, v_s) is determined by the signs of the real part of the two roots namely $\sigma_{1,2}$, whether these are complex

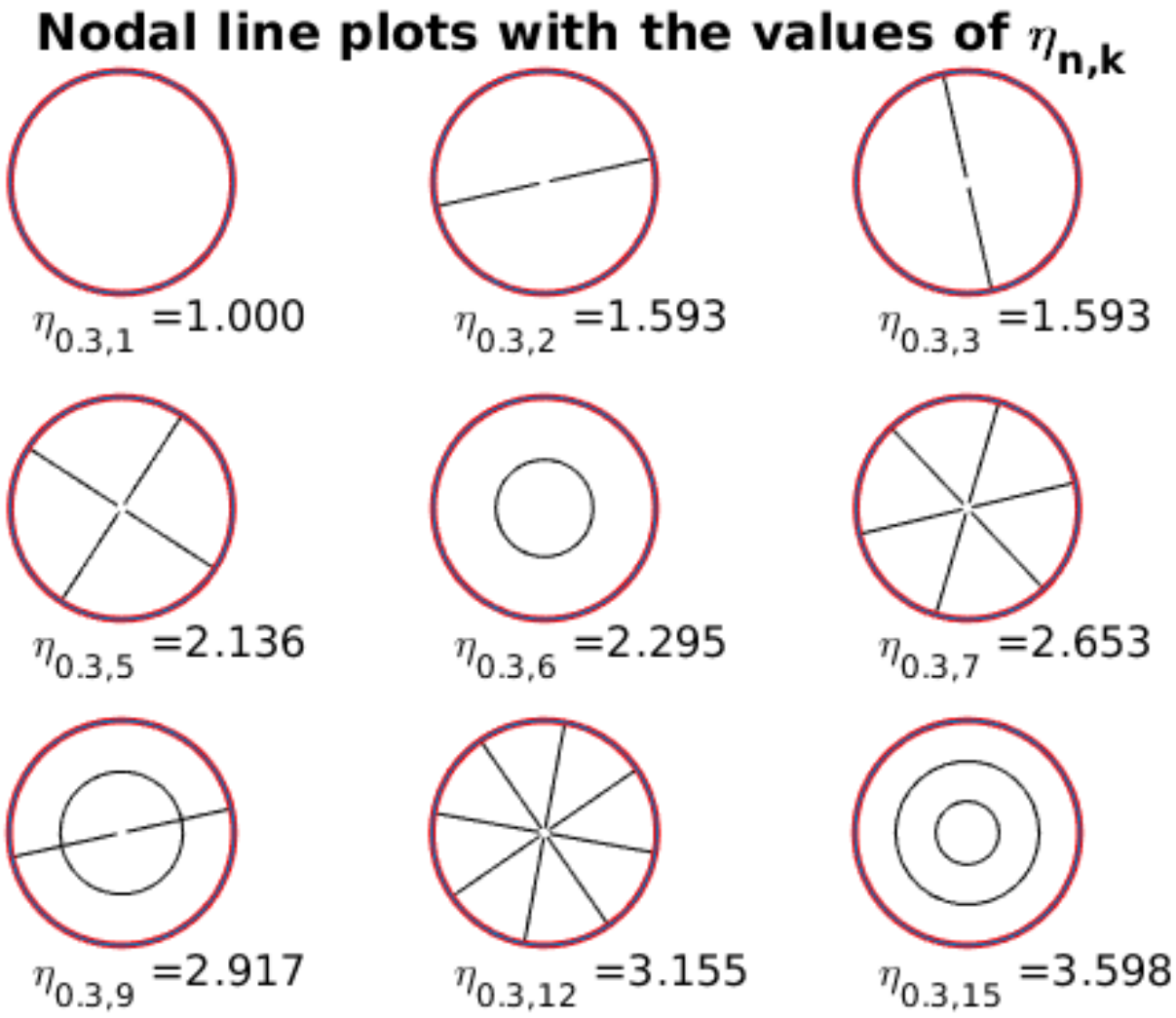

Fig. 2. Nodal lines depiction of the solution and the corresponding eigenvalues satisfying problem (4).

or real.

4. Parameter spaces and bifurcation analysis

Bifurcation analysis of system (1) is better conducted when the parameter plane $(\alpha, \beta) \in \mathbb{R}^2_+$ is appropriately partitioned for both of the cases when $\sigma_{1,2} \in \mathbb{C}\backslash\mathbb{R}$ as well as when $\sigma_{1,2} \in \mathbb{R}$. To obtain such a partition on the parameter plane, it is required to find the equations of the partitioning curves and these can be found through a detailed analysis of the expression for $\sigma_{1,2}$, which in turn requires to explore the domains of $\mathcal{T}$ and $\mathcal{D}$.

4.1. *Equations of the partitioning curves*

Starting with the curve on the parameter plane $(\alpha, \beta) \in \mathbb{R}^2_+$ that forms a boundary for the region that corresponds to eigenvalues $\sigma_{1,2}$ containing non-zero imaginary part. It must be noted that the only possibility through which $\sigma_{1,2}$ can have a non-zero imaginary part is if the inequality $\mathcal{T}^2 - 4\mathcal{D} < 0$ is true. It means that those parameter values α and β satisfying the equation $\mathcal{T}^2(\alpha, \beta) = 4\mathcal{D}(\alpha, \beta)$ must be lying on a partitioning curve that determines the boundary between the region on the parameter plane that corresponds to eigenvalues with non-zero imaginary part and that which corresponds to a pair of real eigenvalues. We

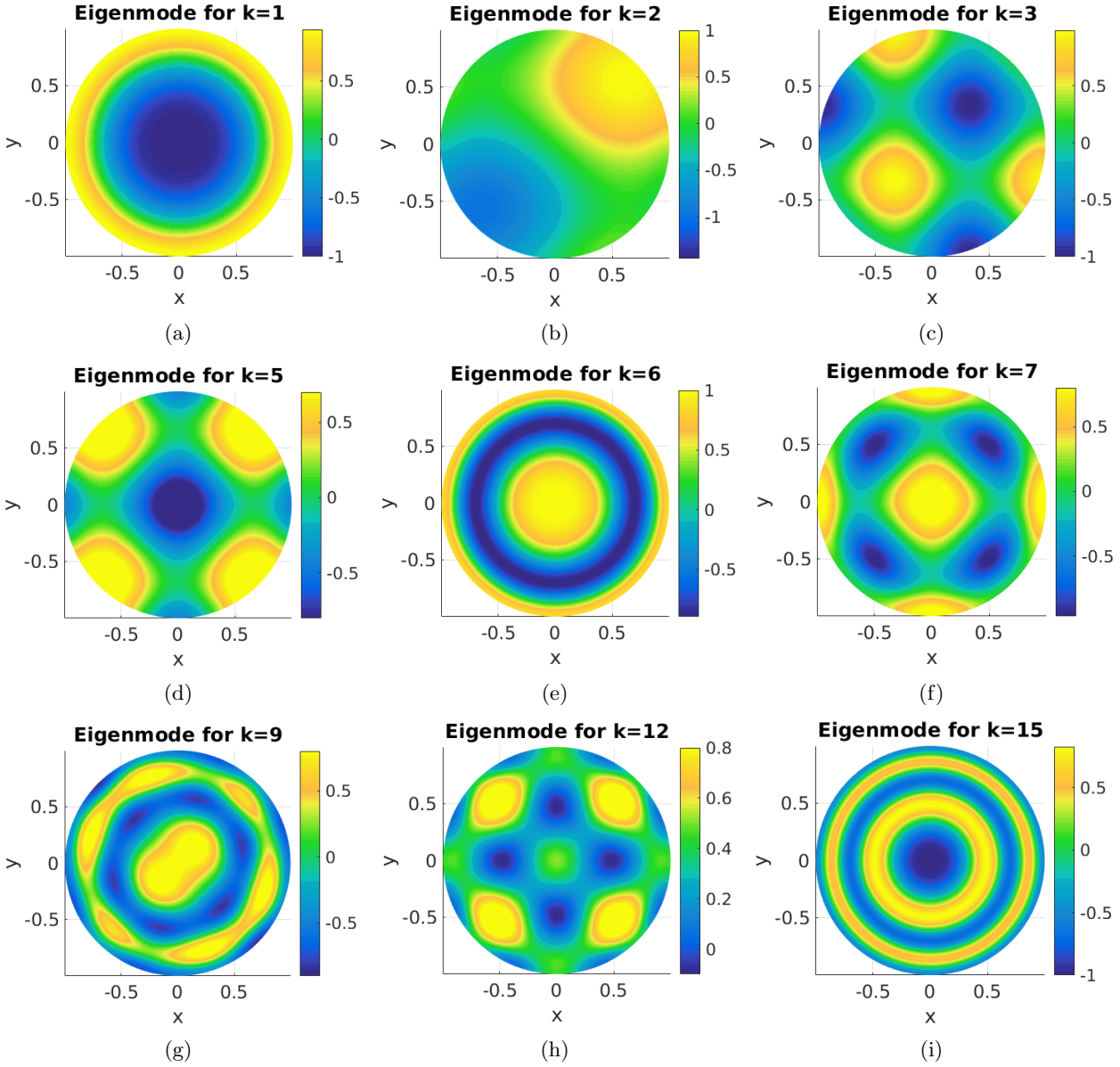

Fig. 3. Colour encoded phaseplots of $w(r,\theta)$ for different values of k indicated in each subtitle.

therefore, state that the set of points on the parameter plane $(\alpha,\beta)\in\mathbb{R}^2_+$ satisfying the implicit equation

$$\Big(\gamma\frac{\beta-\alpha-(\beta+\alpha)^3}{\beta+\alpha}-(d+1)\eta_{n,k}^2\Big)^2 =4\Big(\big(\gamma\frac{\beta-\alpha}{\beta+\alpha}-\eta_{n,k}^2\big)\big(-\gamma(\beta+\alpha)^2 -(d+1)\eta_{n,k}^2\big)+2\gamma^2\beta(\beta+\alpha)\Big), \tag{17}$$

forms the partitioning curve between the region that corresponds to a real pair of $\sigma_{1,2}$ and that corresponding to a complex conjugate pair of $\sigma_{1,2}$. For the solution of (17) refer to Section 5, where a numerical method is employed to find combinations of $\alpha,\beta\in\mathbb{R}_+$ on the plane $(\alpha,\beta)\in\mathbb{R}^2_+$ satisfying (17). The second curve that partitions the bifurcation plane $(\alpha,\beta)\in\mathbb{R}^2_+$ satisfies

$$\gamma\frac{\beta-\alpha-(\beta+\alpha)^3}{\beta+\alpha}=(d+1)\eta_{n,k}^2, \tag{18}$$

with the assumption that $\mathcal{D}(\alpha,\beta) > 0$. This partition occurs within the region corresponding to $\sigma_{1,2}$ containing non-zero imaginary part, because Equation (18) entails that $\mathrm{Re}(\sigma_{1,2}) = 0$.

4.1.1. *Analysis for the case of complex eigenvalues*

Before determining the region with complex eigenvalues on the admissible parameter plane $(\alpha,\beta) \in \mathbb{R}^2_+$ using a numerical treatment of (17), the real part of $\sigma_{1,2}$ is investigated analytically, when it is a complex conjugate pair. It can be noted that $\sigma_{1,2}$ can only become a pair of complex roots, if (α,β) satisfies the inequality

$$\mathcal{T}^2(\alpha,\beta) - 4\mathcal{D}(\alpha,\beta) < 0. \tag{19}$$

Given that (19) is satisfied, then the stability of the uniform steady steady state (u_s, v_s) is decided purely by the sign of the real part of $\sigma_{1,2}$, which is the expression

$$\mathrm{Re}(\sigma_{1,2}) = \frac{1}{2}\Big(\gamma\frac{\beta-\alpha-(\beta+\alpha)^3}{\beta+\alpha} - (d+1)\eta^2_{n,k}\Big). \tag{20}$$

If the sign of the expression given by (20) is negative, simultaneously with assumption (19) satisfied, then it can be predicted that no choice of parameters can cause temporal instability in the dynamics of system (1). Therefore, under the assumption (19), if the dynamics of system (1) do exhibit diffusion-driven instability, it will be restricted to spatially periodic behaviour only, which uniformly converges to a temporal steady state, consequently one obtains spatial pattern that is invariant in time. The sign of the expression given in (20) is further investigated to derive from it, relations between the parameter ρ controlling the domain size and reaction-diffusion rates denoted by γ and d respectively. Given that assumption (19) is satisfied then the sign of expression (20) is negative if parameters α, β, γ and d satisfy the inequality

$$\frac{\beta-\alpha-(\beta+\alpha)^3}{\beta+\alpha} < \frac{(d+1)\eta^2_{n,k}}{\gamma}, \tag{21}$$

with $\eta^2_{n,k}$ defined by (13). Note that the expression on the left hand-side of (21) is a bounded quantity by the constant value of 1 [W. Sarfaraz, A. Madzvamuse , 2017], for all the admissible choices of $(\alpha,\beta) \in \mathbb{R}_+$, therefore, substituting for $\eta^2_{1,2}$ in expression (13) and rearranging, it can be obtained that for inequality (21) to remain true, it induces a restriction on the value of ρ^2, which is of the form

$$\rho^2 < \frac{4(d+1)(2k+1)(n+2k+1)(n+4k)}{\gamma(n+4k+2)}. \tag{22}$$

Inequality (22) conversely implies that so long as the radius ρ of the disk shape domain Ω satisfies (22), then the dynamics of system (1) is guaranteed to exhibit global temporal stability, which also means that any possible instability in the dynamics must be restricted to spatial periodicity or spatial pattern. The formal proof of this claim is presented in Theorem 2. This type of instability concerning space and not time is referred to as *Turing instability* [J. D. Murray , 2013; L. E. Keshet , 2005]. On the other hand assuming that (19) is satisfied and using the upper bound of the quantity on the left hand-side of (21) with $\eta^2_{n,k}$ as defined in (13), it can be shown that a necessary condition for the sign of expression (20) to become positive is for ρ to satisfy the inequality

$$\rho^2 \geq \frac{4(d+1)(2k+1)(n+2k+1)(n+4k)}{\gamma(n+4k+2)}. \tag{23}$$

Conditions (22) and (23) both have quantitative influence on the location and topology of the partitioning curves obtained from the numerical solutions of (17) and (18) in the admissible parameter plane, namely $(\alpha,\beta) \in \mathbb{R}^2_+$. System (1) is restricted from any type of temporal bifurcation if the radius ρ of the disk shape domain Ω is related to the reaction-diffusion parameters γ and d, through inequality (22). It also means that on a disk shape domain Ω with radius ρ satisfying (22), the dynamics of system (1), either exhibit spatially periodic pattern or no pattern at all, both of which are globally stable in time. If the dynamics of a system become unstable along the time axis and exhibits temporal periodicity, then the system is said

to undergo *Hopf bifurcation* [L. Perko , 1996; J. D. Murray , 2013; Y. Fengji, W. Junjie, S. Junping , 2009; M. A. J. Chaplain, M. Ganish, I. G. Graham , 2001]. If the real part of a pair of complex eigenvalues become zero, then the system is expected to exhibit oscillations with orbital periodicity. This behaviour is known as *transcritical bifurcation* [J. D. Murray , 2013; M. A. J. Chaplain, M. Ganish, I. G. Graham , 2001; Y. Fengji, W. Junjie, S. Junping , 2009]. The consequences of the restriction on ρ in the sense of bifurcation analysis means that, whenever the radius ρ of a disk-shape domain is bounded by (22) in terms of γ and d, then the dynamics of system (1) is guaranteed to forbid *Hopf* and *transcritical bifurcations*, only allowing for *Turing instability* to occur. If system (1) allows only Turing type instability to occur under condition (22), it indicates that the eigenvalues $\sigma_{1,2}$ only become positive, when they are a pair of real values with zero imaginary parts. Therefore, it is also an indication that diffusion-driven instability is still possible, but it just becomes strictly spatial with (22) satisfied. If the values of parameters γ and d are chosen such that inequality (23) is satisfied, then the possibility of all three types of diffusion-driven instabilities exist on the admissible parameter plane $(\alpha, \beta) \in \mathbb{R}^2_+$, namely Turing, Hopf and transcritical types of bifurcations. The influence from the area of Ω through the relationship (23) of ρ with the reaction-diffusion rates namely γ and d is summarised in Theorem 2 with a brief sketch of the proof.

Theorem 2 [Hopf or transcritical bifurcation]. *Let u and v satisfy the non-dimensional reaction-diffusion system with activator-depleted reaction kinetics (1) on a disk-shape domain $\Omega \subset \mathbb{R}^2$ with radius ρ and positive real parameters γ, d, α and β. For the system to exhibit Hopf or transcritical bifurcation in the neighbourhood of the unique steady state (u_s, v_s), the necessary condition on the radius ρ of $\Omega \subset \mathbb{R}^2$ is that it must be sufficiently large satisfying* (23) *where $n \in \mathbb{R}\backslash\frac{1}{2}\mathbb{Z}$ is the associated order of the Bessel's equations and k is any positive integer.*

Proof. Consider the real part of $\sigma_{1,2}$, which is precisely given by $\frac{1}{2}\mathcal{T}(\alpha, \beta)$ under the assumption that the admissible choice of parameters $\alpha, \beta \in \mathbb{R}_+$ satisfy (19). When $\sigma_{1,2} \in \mathbb{C}\backslash\mathbb{R}$, then the stability of the uniform steady state (u_s, v_s) is precisely determined by the sign of $\mathcal{T}(\alpha, \beta)$, which is given by

$$\mathcal{T}(\alpha, \beta) = \gamma\frac{\beta - \alpha - (\beta + \alpha)^3}{\beta + \alpha} - (d + 1)\eta^2_{n,k}. \tag{24}$$

System (1) undergoes Hopf or transcritical bifurcation if $\mathcal{T}(\alpha, \beta) \geq 0$, given that the strict inequality (19) is satisfied, which can only hold true if $\mathcal{D}(\alpha, \beta) > 0$. In (24) $\eta^2_{n,k}$ is given by

$$\eta^2_{n,k} = \frac{4(2k + 1)(n + 2k + 1)(n + 4k)}{\rho^2(n + 4k + 2)}, \tag{25}$$

where $n \in \mathbb{R}\backslash\frac{1}{2}\mathbb{Z}$ is the order of the associated Bessel's equation and $k \in \mathbb{N}$ is any positive integer. To show the condition on ρ for Hopf or transcritical bifurcation, one may substitute (25) into (24) and requiring the resulting quantity to be non-negative, which yields the inequality

$$\gamma\frac{\beta - \alpha - (\beta + \alpha)^3}{\beta + \alpha} \geq \frac{4(d + 1)(2k + 1)(n + 2k + 1)(n + 4k)}{\rho^2(n + 4k + 2)}. \tag{26}$$

Noting that the left hand-side of (26) can be written as the difference between two non-negative functions $f_1(\alpha, \beta)$ and $f_2(\alpha, \beta)$ in the form $\gamma\big(f_1(\alpha, \beta) - f_2(\alpha, \beta)\big)$, where f_1 and f_2 are given by

$$f_1(\alpha, \beta) = \frac{\beta}{\alpha + \beta}, \qquad f_2(\alpha, \beta) = \frac{\alpha + (\alpha + \beta)^3}{\alpha + \beta}. \tag{27}$$

In order to find what this inequality induces on the relationship between parameters γ, d and ρ, it is essential to analyse the supremum and infemum of $f_1(\alpha, \beta)$ and $f_2(\alpha, \beta)$ within their respective domains which is $(\alpha, \beta) \in [0, \infty) \times [0, \infty)$. It can be easily shown that $f_1(\alpha, \beta)$ is bounded below and above in the domain $(\alpha, \beta) \in [0, \infty) \times [0, \infty)$ with $\sup_{\alpha,\beta\in\mathbb{R}_+} f_1(\alpha, \beta) = 1$, and $\inf_{\alpha,\beta\in\mathbb{R}_+} f_1(\alpha, \beta) = 0$ for all $\alpha, \beta \in \mathbb{R}_+$. Similarly considering the expression for $f_2(\alpha, \beta)$, then the $\sup_{\alpha,\beta\in\mathbb{R}_+} f_2(\alpha, \beta) = \infty$, and the $\inf_{\alpha,\beta\in\mathbb{R}_+} f_2(\alpha, \beta) = 0$, for all $\alpha, \beta \in \mathbb{R}_+$. Since the ranges of both $f_1(\alpha, \beta)$ and $f_2(\alpha, \beta)$ are non-negative within their respective

domains, therefore the supremum of their difference is determined by the supremum of the function with positive sign, which is $\sup_{\alpha,\beta\in\mathbb{R}_+} f_1(\alpha,\beta) = 1$. Therefore, inequality (26) takes the form

$$\begin{aligned}\frac{4(d+1)(2k+1)(n+2k+1)(n+4k)}{\rho^2(n+4k+2)} &\leq \gamma\frac{\beta-\alpha-(\beta+\alpha)^3}{\beta+\alpha}\\ &\leq \gamma \sup_{\alpha,\beta\in\mathbb{R}_+}\big(f_1(\alpha,\beta)-f_2(\alpha,\beta)\big)\\ &= \gamma \sup_{\alpha,\beta\in\mathbb{R}_+} f_1(\alpha,\beta) = \gamma,\end{aligned} \tag{28}$$

which by rearranging and writing the inequality for ρ in terms of everything else, yields the desired statement of Theorem 2, which is condition (23). ■

4.1.2. *Analysis for the case of real eigenvalues*

The eigenvalues $\sigma_{1,2}$ are both real if

$$\mathcal{T}^2(\alpha,\beta) \geq 4\mathcal{D}(\alpha,\beta). \tag{29}$$

The equal case of (29) is looked at first, where we have

$$\mathcal{T}^2(\alpha,\beta) = 4\mathcal{D}(\alpha,\beta), \tag{30}$$

hence the roots are repeated real values of the form $\sigma_1 = \sigma_2 \in \mathbb{R}$, given by

$$\sigma_1 = \sigma_2 = \frac{1}{2}\Big(\gamma\frac{\beta-\alpha-(\beta+\alpha)^3}{\beta+\alpha} - \frac{4(d+1)(2k+1)(n+2k+1)(n+4k)}{\rho^2(n+4k+2)}\Big). \tag{31}$$

The repeated root is positive provided that ρ satisfies

$$\rho > 2\sqrt{\frac{(\alpha+\beta)(d+1)(2k+1)(n+2k+1)(n+4k)}{\gamma(\beta-\alpha-(\alpha+\beta)^3)(n+4k+2)}}. \tag{32}$$

Otherwise the expression given by (31) can be easily shown to be negative if the radius ρ of the disk-shape domain Ω does not satisfy the strict inequality (32). To ensure that the radius ρ of Ω is not compared against an imaginary number, we impose the following restriction

$$\beta > \alpha + (\beta+\alpha)^3. \tag{33}$$

It must be noted that (23) is a sharper version of (32) in the sense that the curve satisfying (30) subject to condition (32) must be the one forming the boundary of the region on the admissible parameter plane, that corresponds to complex eigenvalues $\sigma_{1,2}$ with positive real parts, which is the region for Hopf bifurcation. Next we state and prove Theorem 3 associated with diffusion-driven instability.

Theorem 3 [Turing type diffusion-driven instability]. *Let u and v satisfy the non-dimensional reaction-diffusion system with activator-depleted reaction kinetics (1) on a disk-shape domain $\Omega \subset \mathbb{R}^2$ with radius ρ and positive real parameters γ, d, α and β. Given that the radius ρ of domain $\Omega \subset \mathbb{R}^2$ satisfy*

$$\rho < 2\sqrt{\frac{(d+1)(2k+1)(n+2k+1)(n+4k)}{\gamma(n+4k+2)}}, \tag{34}$$

where $n \in \mathbb{R}\backslash\frac{1}{2}\mathbb{Z}$ is the associated order of the Bessel's equations and k is any positive integer, then for all $\alpha,\beta \in \mathbb{R}_+$ in the neighbourhood of the unique steady state (u_s, v_s) the diffusion driven instability is restricted to Turing type only, forbidding the existence of Hopf and transcritical bifurcations.

Proof. The strategy of this proof is through detailed analysis of the real part of the eigenvalues of the linearised system, when the eigenvalues are a complex conjugate pair. This can be done through studying the surface $\mathcal{T}(\alpha,\beta)$, and finding that it has a unique extremum point at $(0,0)$. The method of the second derivative test and Hessian matrix is used to determine the type of this extremum. Upon finding its type,

then the monotonicity of $\mathcal{T}(\alpha, \beta)$ is analysed in the neighbourhood of the extremum point in both directions α and β. The monotonicity analysis and the type of the extremum leads to proving the claim of the theorem. For the sake of brevity, we omit the technical details and refer the reader to [W. Sarfaraz, A. Madzvamuse , 2017] where a similar approach was used for rectangular domains. ■

It must be noted that if both eigenvalues are negative real values and distinct, then the system is spatially as well as temporally stable, the dynamics will achieve no patterns, hence the system returns to the uniform constant steady state (u_s, v_s) as time grows, [see Section 6 Fig. 11 (a)] with no effect from diffusion. If the eigenvalues are both real with different signs, then the type of instability caused by diffusion is spatially periodic or oscillatory in space, this case corresponds to the steady state becoming a saddle point. If both eigenvalues are positive real values and distinct, then the dynamics are expected to exhibit a spatially periodic pattern, in the form of stripes or spots.

5. Numerical solution of the partitioning curves and numerical verification

This section mainly focuses on simulating the numerical solutions of (17) and (18), furthermore, a pictorial representation of the implicit curves satisfying (17) and (18) on the admissible parameter plane $(\alpha, \beta) \in \mathbb{R}^2_+$ is obtained in light of which the full classification of the admissible parameter plane is presented. Numerical solutions of the implicit partitioning curves satisfying (17) and (18) are computed subject to conditions respectively given by (23) and (34) on the radius ρ of Ω in terms of parameters d and γ. The relationship between radius ρ of the domain and parameters d and γ is shown to be in agreement with theoretical predictions presented.

Using algebraic manipulation, expanding the brackets and rearranging one can easily show that equation (17) can be written as a six degree implicit polynomial in the variable β, where the coefficients of such polynomial depend on all the remaining parameters namely α, d, γ and the eigenvalues $\eta^2_{n,k}$ of the diffusion operator $\triangle_p$. Let $\psi(\alpha, \beta)$ denote the six degree polynomial obtained from manipulating and rearranging (17), then the curve satisfying $\psi(\alpha, \beta) = 0$ partitions the bifurcation plane $(\alpha, \beta) \in \mathbb{R}^2_+$ into regions corresponding to real and complex eigenvalues $\sigma_{1,2}$ of the stability matrix corresponding to system (1). The algorithm presented in [G. Dimitriu, R. Stefanescu , 2008] is employed and executed for five different values of d to obtain the solutions of (17) and (18) under conditions (23) and (34) on the radius ρ. The shift and existence of the partitioning curves satisfying (17) and (18) are analysed subject to the variation of parameter d. This relation is in agreement and is a numerical demonstration of the conditions for diffusion-driven instability presented in [A. Madzvamuse, A. H. W. Chung, C. Venkataraman , 2015; W. Sarfaraz, A. Madzvamuse , 2017; J. D. Murray , 2013; L. E. Keshet , 2005]. A trial and error method is used to identify which side of the partitioning curves in Fig. 4, corresponds to complex $\sigma_{1,2}$, where the shift of such regions in the parameter space subject to the same respective variation of d is presented in Fig. 5. Investigating the regions corresponding to complex values for $\sigma_{1,2}$ in Fig. 5, using the numerical solution of the cubic polynomial in β with α fixed, it was found that a sub-partition only exists if the value of ρ satisfies condition (23), with respect to the values of d and γ. This is a numerical verification of Theorem 2. If the values of d and/or γ are changed such that ρ no longer satisfies condition (23), it causes to vanish the existence of a sub-partition, within the region corresponding to complex eigenvalues $\sigma_{1,2}$, which is in agreement with Theorem 3. Under such choices of d and γ, the region of the parameter space corresponding to complex $\sigma_{1,2}$ has no stability partition, therefore, everywhere on this region the real part of $\sigma_{1,2}$ is negative. If parameters α and β are fed into system (1), then the dynamics are expected to exhibit global temporal stability. Fig. 6 shows the regions on the admissible parameter spaces corresponding to complex $\sigma_{1,2} \in \mathbb{C}\backslash\mathbb{R}$ with negative real part. It can be noted that the right hand-side of Fig. 6 portrays exactly the same spaces as shown in the right hand-side of Fig. 5, which is a further verification of Theorem 3. If a condition on ρ is set so that it is large enough to exceed the value on the right hand-side of condition (34), i.e. ρ satisfying (23), only then a sub-partition can emerge within the admissible parameter space corresponding to a complex pair of $\sigma_{1,2}$. This can be observed by comparing the left hand-side of Fig. 6 with the left hand-side of Fig. 5. Fig. 7 shows regions and curves on the bifurcation plane that correspond to temporal periodicity in the dynamics. The plot on left hand-side of Fig. 7 shows the spaces on the admissible parameter plane that correspond to

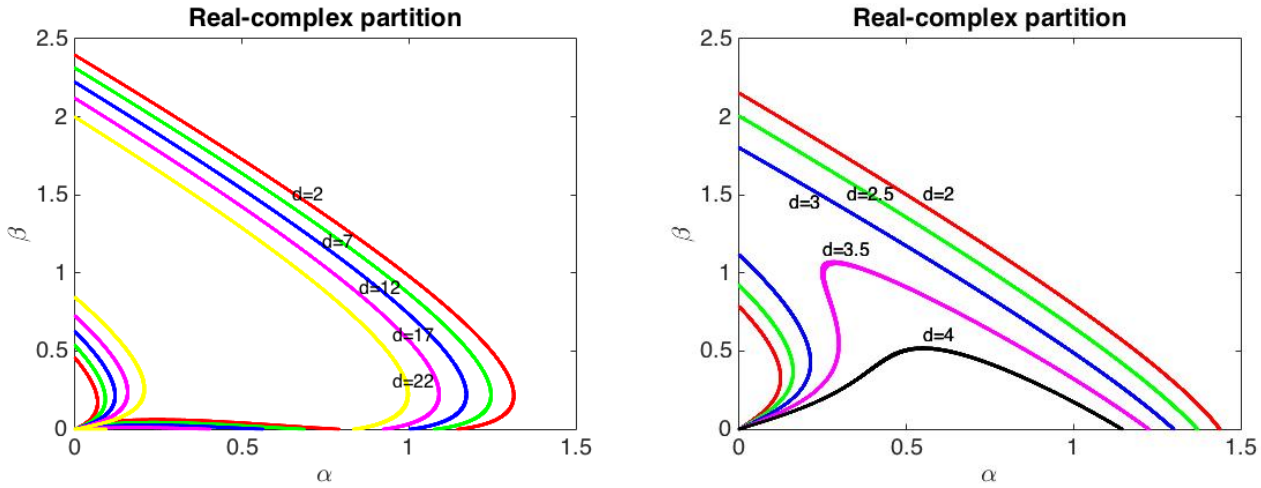

Fig. 4. Partitioning curves satisfying (17) and conditions (23) of Theorem 2 (a) and (34) of Theorem 3 (b), that partition the region corresponding to real $\sigma_{1,2}$ from that corresponding to complex conjugate pair of $\sigma_{1,2}$. The effect of varying d on the solution curves satisfying (17), where ρ is used according to conditions (23) and (34) of Theorems 2 and 3 respectively.

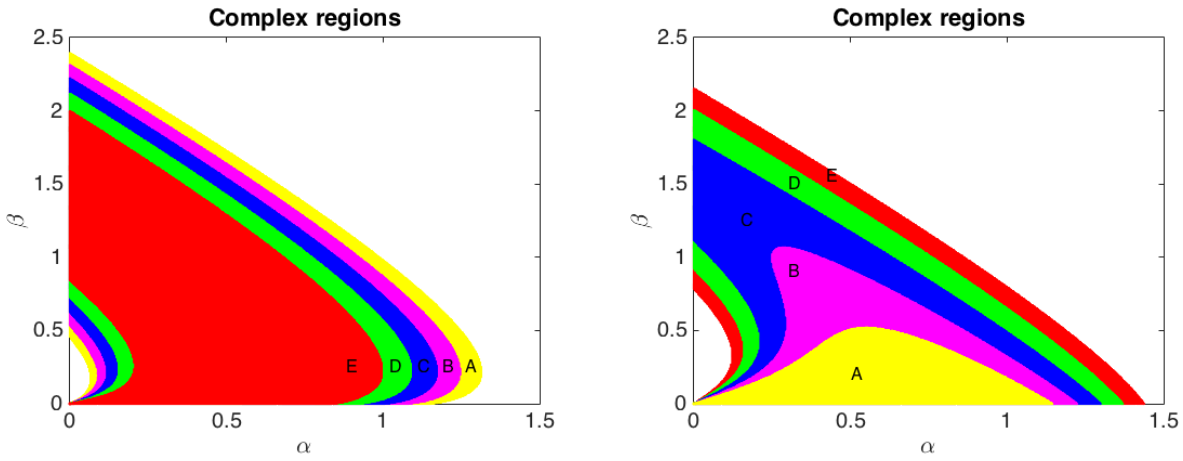

Fig. 5. The shift in parameter spaces corresponding to complex $\sigma_{1,2}$ as a consequence of varying d.

Hopf bifurcation, whereas the spaces in right hand-side of Fig. 7 correspond to transcritical bifurcation in the dynamics of (1).

Fig. 8 shows the shift in the regions that correspond to real pair of $\sigma_{1,2}$ as a consequence of varying d. Bear in mind that the union of spaces given in Fig. 8 and 5 form the top right quadrant of the cartesian plane. The outer partitioning curves of the regions corresponding to complex eigenvalues in Fig. 4, indicate the choice of α and β for which the eigenvalues $\sigma_{1,2}$ is a pair of real repeated negative values, therefore, parameter spaces bounded by these curves corresponds to a pair of distinct negative real values. Parameter choice from these regions corresponds to a global spatio-temporally stable behaviour of the dynamic of system (1). Fig. 9 shows the shift of these spatio-temporal stable regions on the admissible parameter space. Any choice of α and β from these regions will result in the dynamics of system (1) to exhibit global stability in space and in time. The remaining spaces to analyse are those corresponding to diffusion-driven instability of Turing type under conditions (23) and (34) on ρ, when $\sigma_{1,2}$ are a pair of real values with at least one of them positive. This region corresponds to Turing type instability and under both conditions on ρ these regions exist. We know that the diffusion-driven instability can also happen when either σ_1 or σ_2 are positive real. Fig. 10 shows the shift of those regions corresponding to Turing type instability and it can be observed that as d increases, the region in the parameter space enlarges.

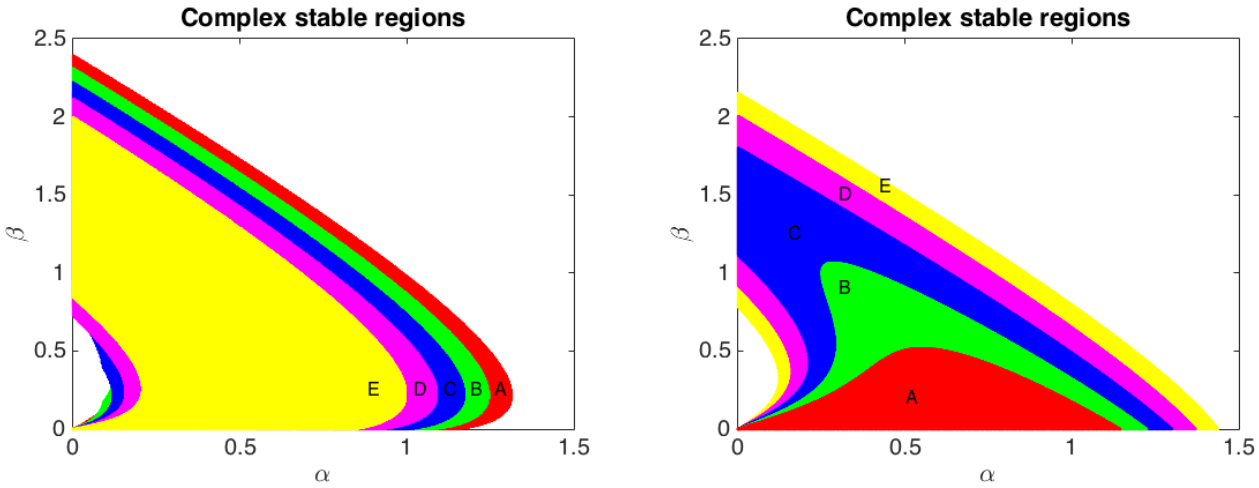

Fig. 6. The shift in parameter spaces corresponding to complex $\sigma_{1,2}$ with negative real parts as a consequence of varying d.

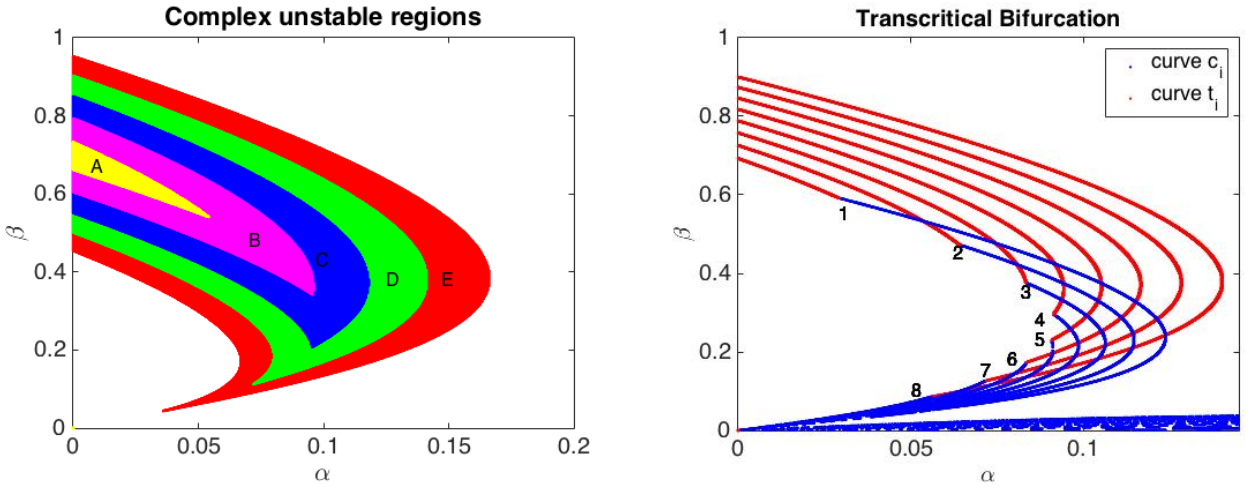

Fig. 7. Regions in the Figure on the left correspond to Hopf bifurcation and curves t_i (on the right) correspond to transcritical bifurcation. When ρ satisfies condition (34), then no values of α and β give rise to temporal instability in system (1).

Stability of USS (u_s, v_s)			Stable regions		Unstable regions		
Types of USS (u_s, v_s)			Node	Spiral	Turing-instability	Hopf bifurcation	Transcritical bifurcation
Figure index			Fig. 9 left	Fig. 6 left	Fig. 10 left	Fig. 7 left	Fig. 7 right
Theorem 2	ρ satisfying (23)	$\sigma_{1,2}$ / (d,γ,ρ,n)	$0 > \sigma_{1,2} \in \mathbb{R}$	$\sigma_{1,2} \in \mathbb{C}\backslash\mathbb{R}, \mathrm{Re}(\sigma) < 0$	$0 < \sigma_1 \in \mathbb{R}$ or $0 < \sigma_2 \in \mathbb{R}$	$\sigma_{1,2} \in \mathbb{C}\backslash\mathbb{R}$, $\mathrm{Re}(\sigma_{1,2}) > 0$	$\sigma_{1,2} \in \mathbb{C}\backslash\mathbb{R}$, $\mathrm{Re}(\sigma_{1,2}) = 0$
		$(2.0, 1, 35, 1.7)$	A	$A \cup B \cup C \cup D \cup E$	E	$A \cup B \cup C \cup D \cup E$	t_8
		$(7.0, 1, 35, 1.7)$	$A \cup B$	$B \cup C \cup D \cup E$	$E \cup D$	$A \cup B \cup C \cup D$	t_6
		$(12, 1, 35, 1.7)$	$A \cup B \cup C$	$C \cup D \cup E$	$E \cup D \cup C$	$A \cup B \cup C$	t_3
		$(17, 1, 35, 1.7)$	$A \cup B \cup C \cup D$	$D \cup E$	$E \cup D \cup C \cup B$	$A \cup B$	t_2
		$(22, 1, 35, 1.7)$	$A \cup B \cup C \cup D \cup E$	E	$E \cup D \cup C \cup B \cup A$	A	t_1
Figure index			Fig. 9 right	Fig. 6 right	Fig. 10 right	Fig. 7 right	Fig. 6 right
Theorem 3	ρ satisfying (34)	$\sigma_{1,2}$ / (d,γ,ρ,n)	$0 > \sigma_{1,2} \in \mathbb{R}$	$\sigma_{1,2} \in \mathbb{C}\backslash\mathbb{R}, \mathrm{Re}(\sigma) < 0$	$0 < \sigma_1 \in \mathbb{R}$ or $0 < \sigma_2 \in \mathbb{R}$	$\sigma_{1,2} \in \mathbb{C}\backslash\mathbb{R}$, $\mathrm{Re}(\sigma_{1,2}) > 0$	$\sigma_{1,2} \in \mathbb{C}\backslash\mathbb{R}$, $\mathrm{Re}(\sigma_{1,2}) = 0$
		$(2.0, 1, 10, 1.7)$	E	$A \cup B \cup C \cup D \cup E$	A	$\emptyset$	$\emptyset$
		$(2.5, 1, 10, 1.7)$	$E \cup D$	$A \cup B \cup C \cup D$	$A \cup B$	$\emptyset$	$\emptyset$
		$(3.0, 1, 10, 1.7)$	$E \cup D \cup C$	$A \cup B \cup C$	$A \cup B \cup C$	$\emptyset$	$\emptyset$
		$(3.5, 1, 10, 1.7)$	$E \cup D \cup C \cup B$	$A \cup B$	$A \cup B \cup C \cup D$	$\emptyset$	$\emptyset$
		$(4.0, 1, 10, 1.7)$	$E \cup D \cup C \cup B \cup A$	A	$A \cup B \cup C \cup D \cup E$	$\emptyset$	$\emptyset$

6. Finite element solutions of RDS

To verify numerically the classification of parameter spaces proposed by Theorems 2 and 3, the reaction-diffusion system (1) is simulated using the finite element method [R. Barreira, C. M. Elliot, A. Madzvamuse

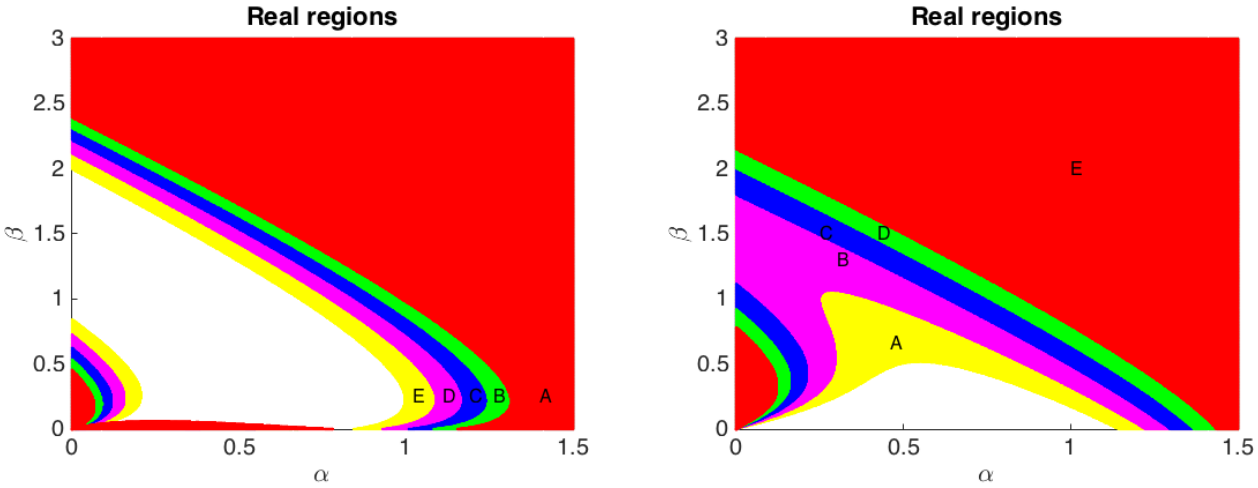

Fig. 8. The shift in parameter spaces corresponding to real $\sigma_{1,2}$ as a consequence of varying d.

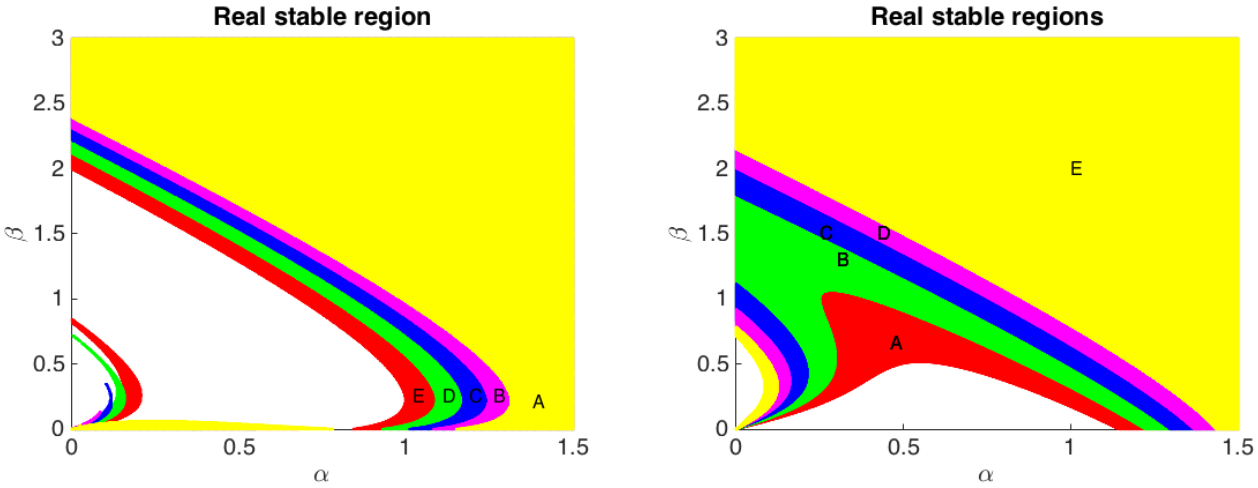

Fig. 9. The shift in parameter spaces corresponding to negative real distinct $\sigma_{1,2}$ as a consequence of varying d.

, 2011; A. Madzvamuse , 2006; O. Lakkis, A. Madzvamuse, C. Venkataraman , 2014; A. Madzvamuse, P. K. Maini, A. J. Wathen , 2005, 2003; A. Schnepf, D. Leitner , 2009; I. M. Smith, D. V. Griffiths , 1988; M. J. Baines , 1994; M. G. Larson, F. Bengzon , 2013] on a unit disk Ω. Due to the curved boundary of Ω, the triangulation is obtained through an application of an iterative algorithm using a technique called *distmesh* [O. Persson , 2015; A. Schnepf, D. Leitner , 2009]. For details on how to generate meshes using *distmesh* we refer the interested reader to the paper by Persson and Strang [O. Persson , 2015; A. Schnepf, D. Leitner , 2009; G. Strang, P. O. Persson , 2004]. Using the *distmesh* algorithm, a unit disk Ω was discretised to obtain a uniform triangulation. Each simulation in this section is performed on a unit disk centred at the origin of cartesian plane, which is discretised by 6327 triangles consisting of 3257 nodes. The initial conditions for each simulation are taken to be small random perturbations in the neighbourhood of the steady state (u_s, v_s) of the form [J. D. Murray , 2013; L. E. Keshet , 2005; W. Sarfaraz, A. Madzvamuse , 2017; A. Madzvamuse, A. H. W. Chung, C. Venkataraman , 2015]

$$\begin{cases} u_0(x,y) = \alpha + \beta + 0.0016\cos(2\pi(x+y)) + 0.01\sum_{i=1}^{8}\cos(i\pi x), \\ v_0(x,y) = \frac{\beta}{(\alpha+\beta)^2} + 0.0016\cos(2\pi(x+y)) + 0.01\sum_{i=1}^{8}\cos(i\pi x). \end{cases} \tag{35}$$

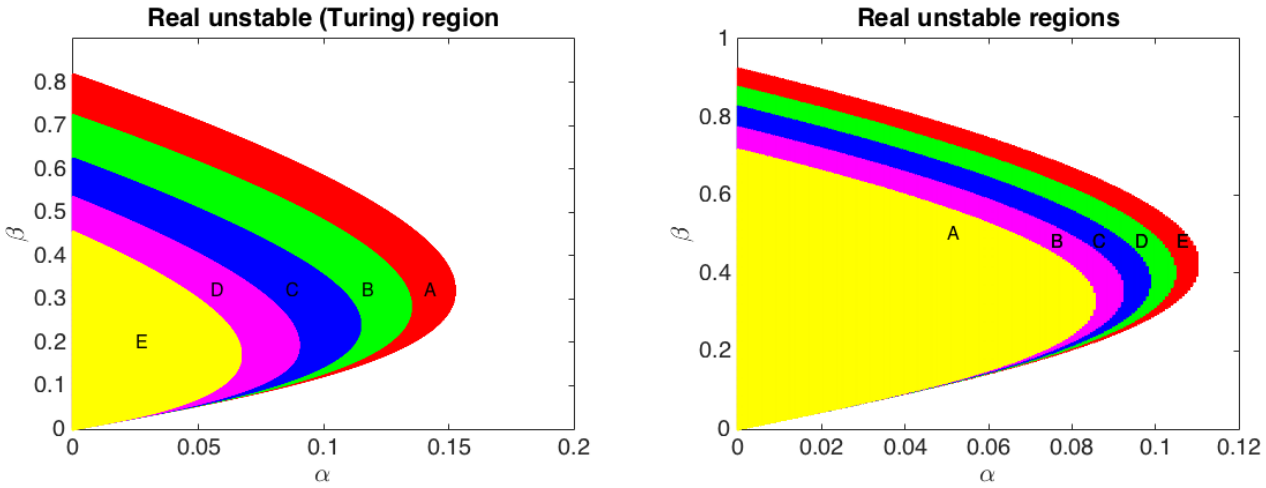

Fig. 10. The shift in parameter spaces corresponding to at least one positive real eigenvalue $\sigma_{1,2}$ as a consequence of varying d.

The choices of parameters α and β are verified from each of the four regions where the dynamics of system (1) exhibit diffusion-driven instability. It proves computationally expensive to vary ρ, therefore in order to satisfy conditions (23) and (34), hence in all our simulations, it suffices to vary the values of d and γ to ensure that a particular condition on the domain size in terms of reaction-diffusion rates is satisfied, whilst keeping the value of radius $\rho = 1$ fixed, which allows us to keep constant the well refined number of degrees of freedom for the mesh. The actual numerical values for each simulation are presented in Table 2. All the simulations were executed for long enough time such that the discrete time derivative of solutions u and v decays to a threshold of 5×10^{-4} in the discrete L_2 norm. We use this measure to study the temporal behaviour of the numerical solutions.

6.1. *Global spatio-temporal stability*

Before demonstrating diffusion-driven instability, a pair of parameter values α and β from the spatio-temporally stable region indicated in Table 1 is used to demonstrate, in Fig. 11 (a), how the dynamics overcome small perturbations and reach the uniform steady state (u_s, v_s) without evolving to any pattern. The uniform convergence to the constant steady state (u_s, v_s) is shown in Fig. 11 (b), through the convergence of the discrete L_2 norm of the discrete time derivatives of the solutions u and v.

6.1.1. *Turing instability for small and large radii*

Fig. 12 shows the evolution of a spatial pattern as a consequence of choosing (α, β) from the Turing region under condition (34) indicated in Fig. 10. Fig. 13 presents a series of three snapshots to show how the spatially periodic pattern is evolved to a Turing type steady state, when parameters α and β are chosen from Turing region and ρ satisfying condition (23), with respect to d and γ. For simulations shown in Fig. 13, parameters α and β are chosen from regions presented in Fig. 10 (a); the dynamics within these regions evolve to a spatial pattern with global temporal stability. It can be noted from Fig. 13 (d), that after the initial pattern is formed, the system is uniformly converging to the spatially periodic steady state. Turing instability is a domain independent phenomena, and only depends on the choice of parameters and the initial conditions. At $t = 6$ the required threshold on the discrete L_2 norm of the discrete time derivatives of the solutions u and v is reached, which can be observed in Fig. 13 (d). The remaining two unstable regions in the admissible parameter space presented in Fig. 7 correspond to spatio-temporal periodicity.

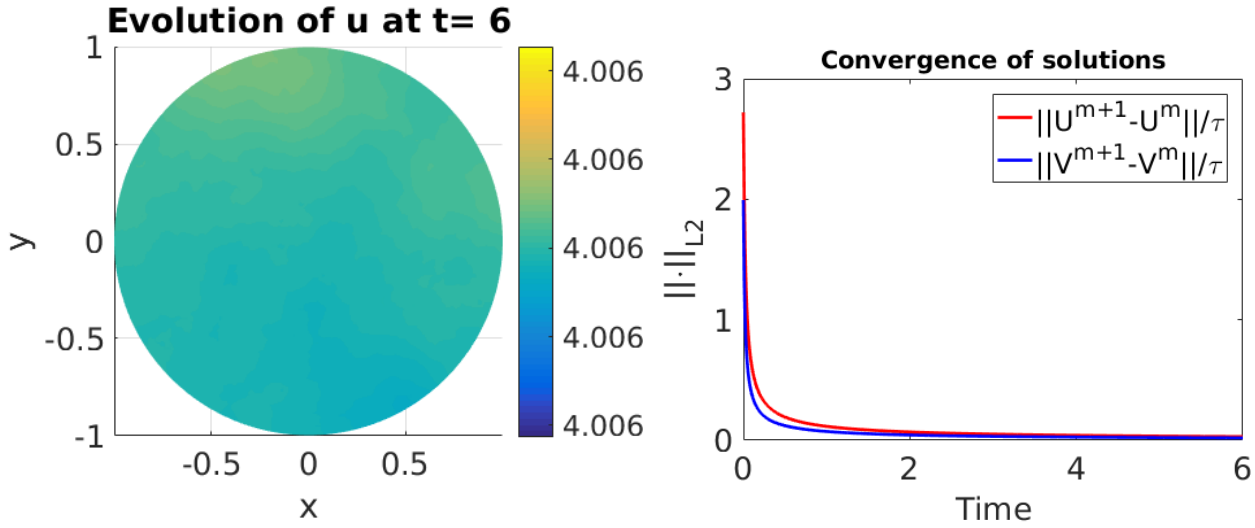

Fig. 11. When ρ is bounded by a combination of d and γ (as shown in Table 2) according to condition (34), then no choice of (α, β) outside Turing-space can trigger instability in the dynamics, hence no pattern emerges.

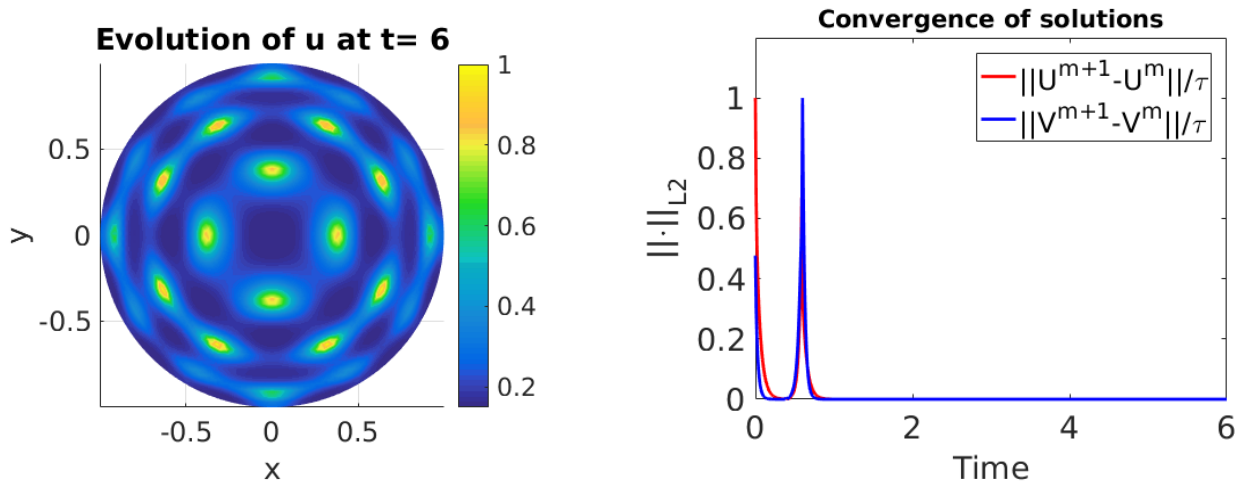

Fig. 12. When ρ is bounded by a combination of d and γ (as shown in Table 2) according to condition (34), then the only admissible pattern is a spatially periodic pattern for (α, β) from the Turing-space.

6.2. *Hopf bifurcation*

Regions presented in Fig. 7 (a) are those corresponding to a complex conjugate pair of eigenvalues with non-zero positive real part. These regions emerge in the admissible parameter space under condition (23) on ρ. Choosing parameters from regions in Fig. 7 (a) admits temporal periodic behaviour in the dynamics of system (1) as shown in Fig. 14. The initial pattern in Fig. 14 (a) is in fact achieved earlier than at $t = 1$, therefore, the temporal gap between the initial and second pattern in Fig. 14 (b) is relatively smaller than the temporal gaps that exist between the second, third and fourth temporal periods. It is worth noting that the temporal period between the successive transitional temporal instabilities from one type of spatial pattern to another grows larger with time. The initial pattern is obtained at around $t \approx 1$, which becomes unstable during the transition to the second temporal period at $t \approx 5$ in Fig. 14 (b). At $t \approx 8$ the system undergoes a third period of instability and reaches a different spatial pattern at $t \approx 12$ shown in Fig. 14 (c). The fourth period of temporal instability is reached at $t \approx 20$, which converges to the fourth temporally-local but spatially periodic steady state at $t \approx 28$ presented in Fig. 14 (d). It follows that when parameters

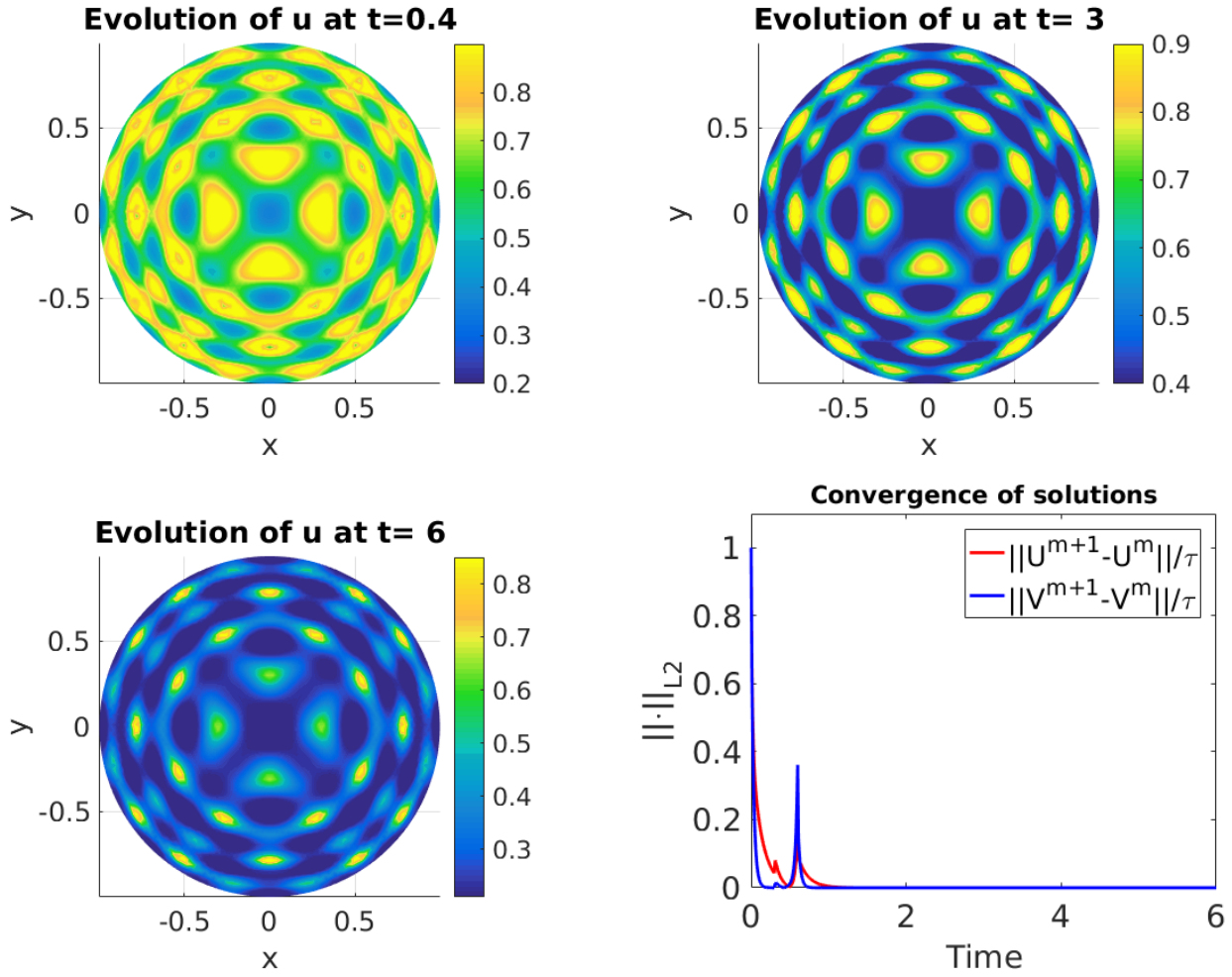

Fig. 13. When ρ is large with respect to the combination of d and γ (as shown in Table 2) according to condition (23), then the dynamics admit spatial diffusion-driven instability for (α, β) from the Turing-space.

are chosen from the Hopf bifurcation region then the temporal gaps in the dynamics of system (1) between successive transitional instabilities from one spatial pattern to another is approximately doubled as time grows. It is speculated that the temporal period-doubling behaviour is connected to the analogy of unstable spiral behaviour in the theory of ordinary differential equations (ODEs) [L. Perko , 1996]. If the eigenvalues of a dynamical system modelled by a set of ODEs is a complex number with positive real part, then the cycles of the corresponding unstable spiral grow larger as time grows. The long-term evolution of temporal instability depends on the magnitude of the real part of $\sigma_{1,2}$. If parameters (α, β) are chosen such that the trace of the stability matrix in (3) is large and yet the discriminant is negative, then the dynamics exhibit long-term temporal periodicity, which means that the frequency of temporal cycles will become smaller. A decaying frequency in temporal cycles means that locally on the time axis, the dynamics may exhibit similar behaviour to that of a temporally stable system, therefore, to observe temporal transition from one spatial pattern to another, we solve the model system for a long time. Fig. 14 (e) shows a visualisation of the transition of such temporal periodicity with a decaying frequency.

6.3. *Transcritical bifurcation*

As stated in Theorem 2, when ρ satisfies condition (23) with respect to d and γ, given that the parameters (α, β) chosen from the curves t_i for $i = 1, ..., 8$ as indicated in Fig. 7 (b), then one may expect the dynamics of system (1) to exhibit spatio-temporal periodic pattern, through a transcritical bifurcation. This kind of

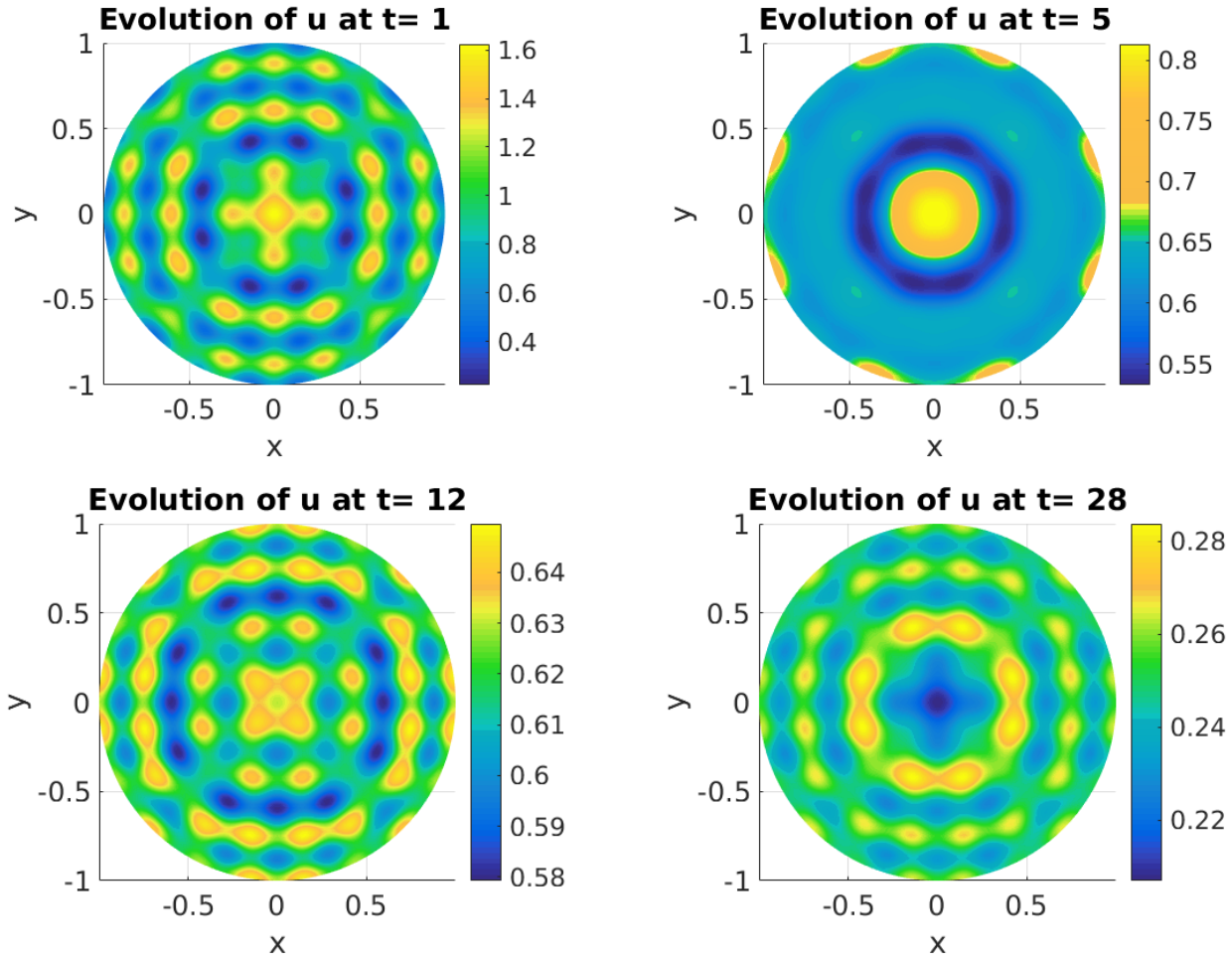

Fig. 14. When ρ is large with respect to the combination of d and γ (as shown in Table 2) according to condition (23), then the dynamics admit spatio-temporal diffusion-driven instability for (α, β) from Hopf bifurcation region presented in Fig. 7 (a).

behaviour in the dynamics is also known as the limit cycles [L. Perko , 1996]. Fig. 17 shows this spatio-temporal periodic behaviour in the evolution of the numerical solution of system (1). This is the case corresponding to parameters that ensure the eigenvalues to be purely imaginary, therefore, it can be observed that the temporal instability occurs with approximately constant periods along the time axis, which verifies the theoretical prediction of the transcritical bifurcation. It is also observed that during the transitional instability from spots in Fig. 17 (a) to the angular stripes in Fig. 17 (b) the peak of the discrete L_2 norm of the discrete time-derivative of the activator u is bigger than that of the inhibitor v. However, when the transitional temporal instability occurs to turn the angular stripes in Fig. 17 (b) into spots in Fig. 17 (c), then the discrete L_2 norm of the time-derivative of the inhibitor v exceeds in magnitude than that of the activator u. This alternating behaviour can be clearly observed in Fig. 17 (e), where in the annotated legend U and V denote the discrete solutions of the activator u and that of the inhibitor v. It can further be understood from Fig. 17 (e), that if (α, β) are chosen from the curves of the transcritical bifurcation given in Fig. 7 (b), then the frequency of temporal periods is predicted to remain constant for all times, resulting in a constant interchanging behaviour between different spatial patterns.

7. Conclusion

Analytical methods were used to derive conditions (23) and (34) on the radius of a disk-shape domain in the context of bifurcation analysis. It was found that Turing instability occurs independent of the size of the radius, whereas temporal bifurcation in the dynamics are domain dependent, in particular under

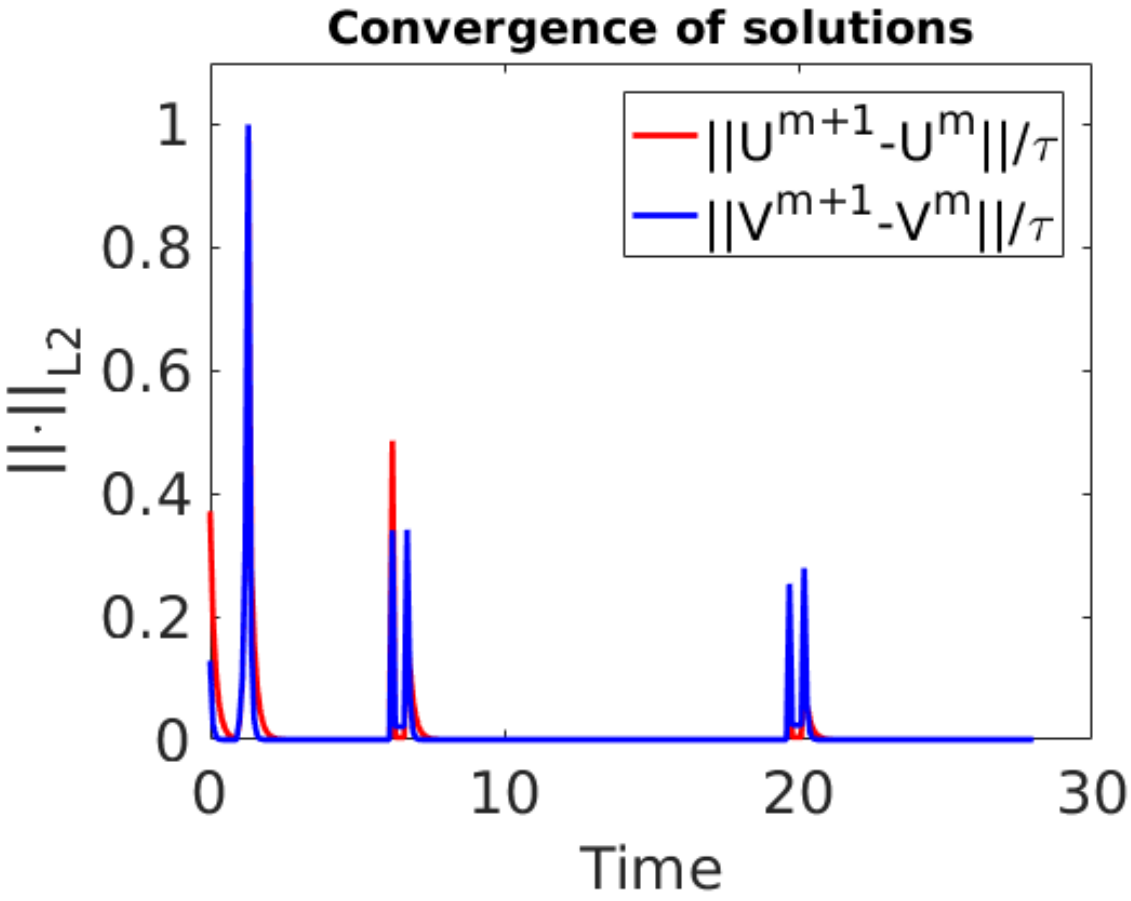

Fig. 15. Spatio-temporal periodicity in the dynamics measured in dicrete L_2 norm of the successive time-step difference of the solutions u and v.

Plot index	Fig. 11	Fig. 12	Fig. 13	Fig. 14	Fig. 17
Instability / Parameters	No instability No pattern	Turing type instability Spatial pattern	Turing type instability Spatial pattern	Hopf bifurcation Spatial and temporal pattern	Transcritical bifurcation Spatial and temporal pattern
(α, β)	$(2, 2)$	$(0.1, 0.5)$	$(0.13, 0.3)$	$(0.15, 0.4)$	$(0.05, 0.7)$
(n, d, γ)	$(2.7, 10, 210)$	$(2.7, 10, 210)$	$(1.7, 6, 450)$	$(1.7, 6, 480)$	$(1.7, 6, 500)$
Condition on Ω	(34)	(34)	(23)	(23)	(23)
Simulation time	6	6	6	28	9
CPU time (sec)	784.24	784.56	784.91	4151.48	1197.66

condition (23). The relationship between reaction-diffusion rates and the radius of a disk-shape domain was established and analytically proven in Theorems 2 and 3. The full parameter space was classified with respect to the stability and types of the uniform steady state. Parameter values from all of the regions were tested and the predicted bifurcation in the dynamics was verified using the finite element method. Spatio-temporal periodicity of Hopf and transcritical types were shown and the corresponding plots of the discrete L_2 norms of the time-derivative of the solutions were obtained to demonstrate the temporal periods of limit cycles and Hopf bifurcation. It was further verified that under certain conditions on the radius of a disk with respect to the reaction-diffusion rates, the instability in the dynamics is restricted to Turing-type only forbidding the existence of a region for temporal bifurcation. A distinction between the transcritical and Hopf bifurcations was numerically established by analysing the temporal periods between transitional instabilities in the dynamics from one spatial pattern to another. The methodology used in the current paper sets an exclusive framework for a strategy to investigate general reaction-diffusion systems on arbitrary geometries. The current work brings together two important and routinely used approaches namely linear stability theory and the numerical computation to obtain robust and complete insight on the

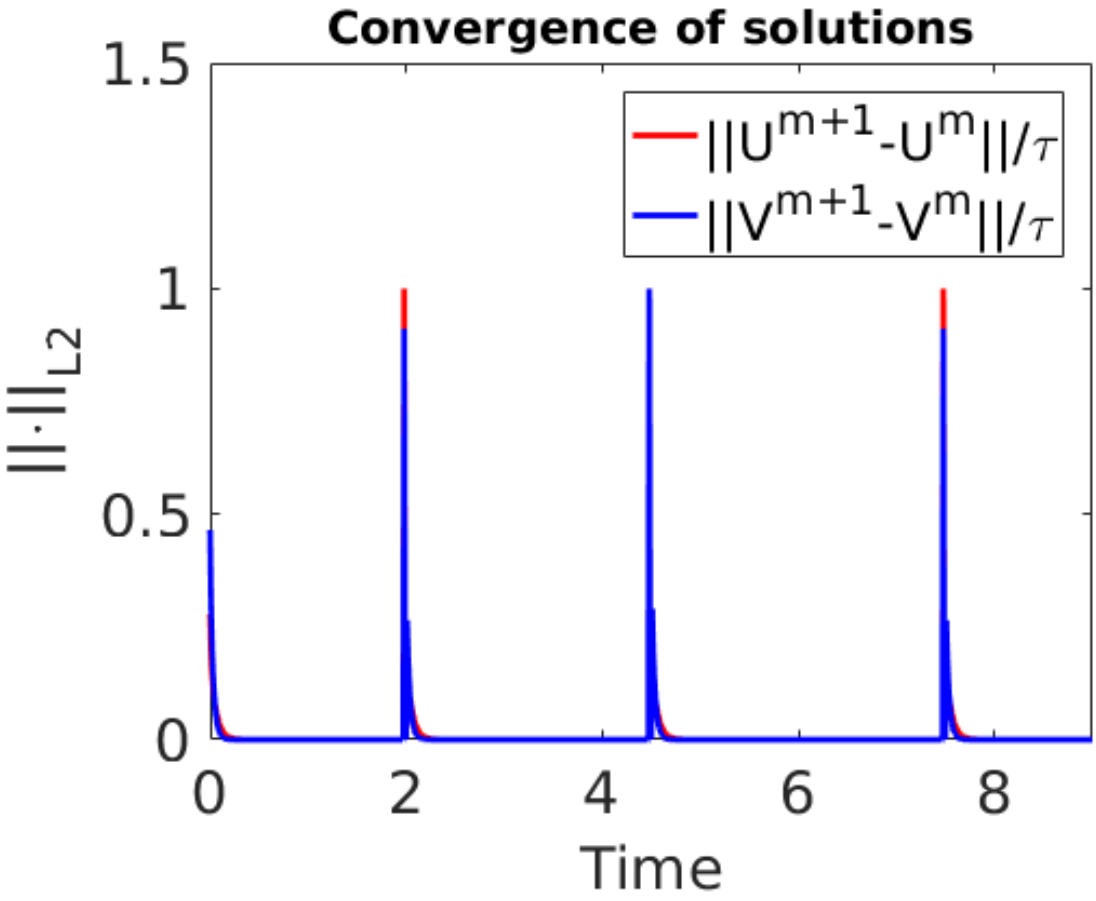

Fig. 16. Plot of the discrete L_2 norm of the discrete time-derivative of u and v showing the spatio-temporal behaviour of the solutions for successive time-steps.

parameter spaces and the influence and role of domain size on the bifurcation theory.

We are currently extending this theoretical framework to study bifurcation analysis for reaction-diffusion systems with cross-diffusion [S. Ghorai, S. Poria , 2016; A. Madzvamuse, H. S. Ndakwo, R. Barreira , 2016]. We want to study or investigate whether the existence of cross-diffusion has any influence on the conditions derived for the domain size in the context of bifurcation analysis with independent diffusion rates. The strategy used in this paper can also be applied to study bulk-surface reaction-diffusion systems on three dimensional domains [A. Madzvamuse, A. H. W. Chung , 2015, 2014; A. Madzvamuse, A. H. W. Chung, C. Venkataraman , 2015; R. Barreira, C. M. Elliot, A. Madzvamuse , 2011] by investigating how the surface area and the volume of three dimensional domains influence the spatio-temporal behaviour of the system. Furthermore, our theoretical and conceptual framework allows us to investigate how continuous domain and surface growth and evolution influences the bifurcation behaviour of the system [M. A. J. Chaplain, M. Ganish, I. G. Graham , 2001; R. Barreira, C. M. Elliot, A. Madzvamuse , 2011; A. Madzvamuse , 2008; C. Venkataraman, O. Lakkis, A. Madzvamuse , 2012; A. Madzvamuse , 2006; C. Venkataraman , 2011]. The strategy of the current work motivates us to investigate whether conditions (23) and (34) continue to influence the dynamics in the presence of continuous domain and surface growth and evolution, or whether beyond a certain threshold of the domain or surface size, these conditions can be invalidated. Here, analytical theory on non-autonomous partial differential equations must be exploited appropriately.

8. Acknowledgments

WS acknowledges support of the School of Mathematical and Physical Sciences Doctoral Training studentship. AM acknowledges support from the Leverhulme Trust Research Project Grant (RPG-2014-149)

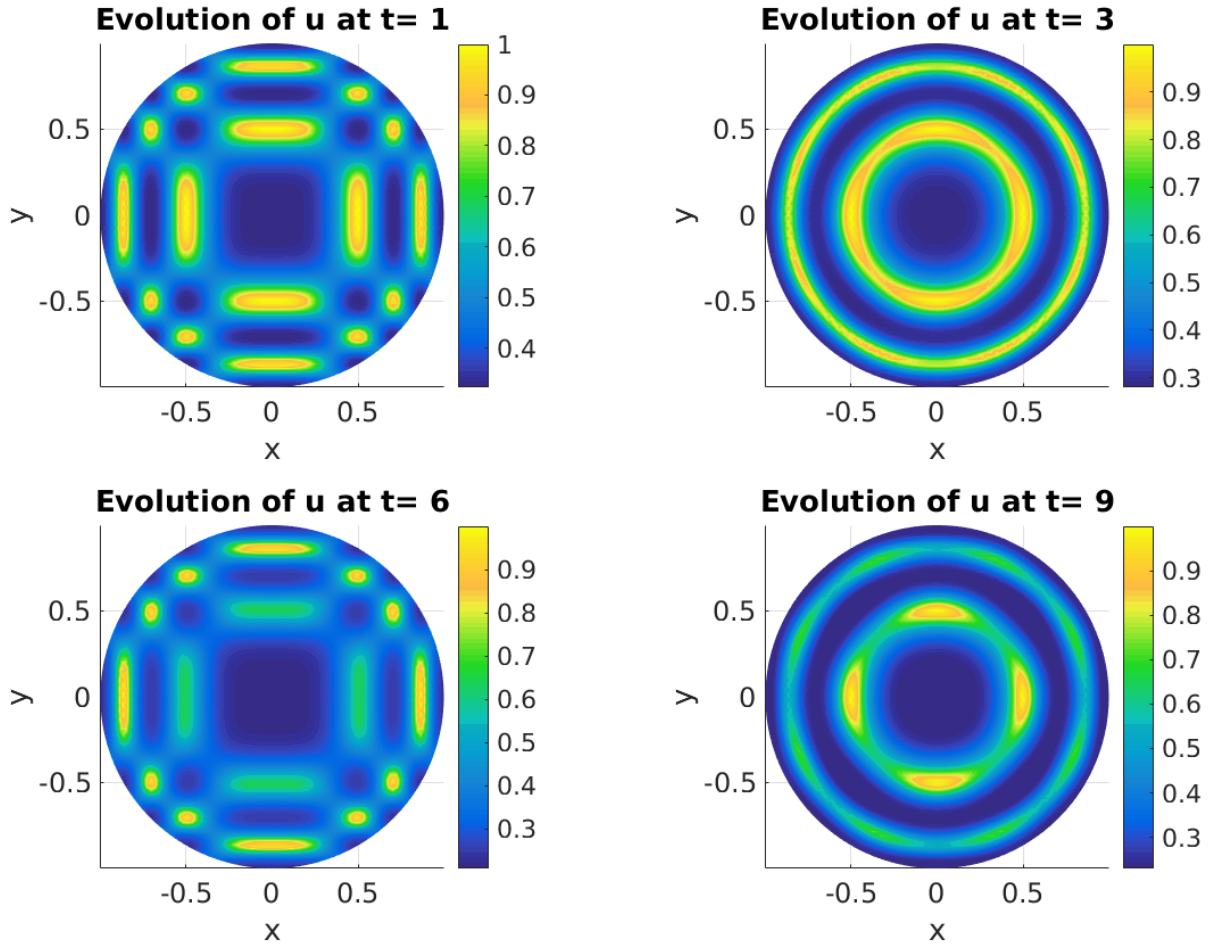

Fig. 17. When ρ is large with respect to the combination of d and γ (as shown in Table 2) according to condition (23), then the dynamics of (1) can also admit spatio-temporal diffusion-driven instability for (α, β) from the transcritical birfucation curves indicated in Fig. 7 (b).

and the European Union's Horizon 2020 research and innovation programme under the Marie Sklodowska-Curie grant agreement No 642866. AM's work was partially supported by the Engineering and Physical Sciences Research Council, UK grant (EP/J016780/1). The authors (WS, AM) thank the Isaac Newton Institute for Mathematical Sciences for its hospitality during the programme (Coupling Geometric PDEs with Physics for Cell Morphology, Motility and Pattern Formation; EPSRC EP/K032208/1). AM was partially supported by a fellowship from the Simons Foundation. AM is a Royal Society Wolfson Research Merit Award Holder, generously supported by the Wolfson Foundation.

References

A. M. Turing [1952] "The chemical basis of morphogenesis," *Philos. Trans. R. Soc. Lond*, **237**, pp. 37–72.

M. A. J. Chaplain, M. Ganish, I. G. Graham [2001] "Spatio-temporal pattern formation on spherical surfaces: Numerical and application to solid tumour growth," *J. Math. Biol*, **42**, pp. 387–432.

A. Madzvamuse, A. H. W. Chung [2015] "The bulk-surface finite element method for reaction-diffusion systems on stationary volumes," *J. FE in Analysis and Design.*, **108**, pp. 1–21.

A. Madzvamuse, A. H. W. Chung [2014] "Fully implicit time-stepping schemes and non-linear solvers for systems of reaction-diffusion equations,"*J. App. Math. Comp.*, **244**, pp. 361–374.

S. Yan., X. Lian, W. Wang, R. K. Upadhyay [2014] "Spatiotemporal dynamics in a delayed diffusive predator model,"*J. App. Math. Comp.*, **224**, pp. 524–534.

R. Barreira, C. M. Elliot, A. Madzvamuse [2011] "The surface finite element method for pattern formation on evolving biological surfaces,"*Online. J. Math. Biol.*, **29**, DOI: 10.1007/s00285-011-0401-0.

S. Ghorai, S. Poria [2016] "Turing pattern induced by cross-diffusion in a predator-prey system in presence of habitat complexity,"*J. Chaos. Solit. Fract.*, **91**, pp. 421–429.

R. Zhang. X. Yu, J. Zhu, A. F. D. Loula [2014] "Direct discontinuous Galerkin method for nonlinear reaction-diffusion systems in pattern formation,"*J. App. Math. Mod.*, **38**, pp. 1612–1621.

A. Madzvamuse [2008] "Stability analysis of reaction-diffusion systems with constant coefficients on growing domains,"*Int. J. Dyn. Diff. Eq.*.

C. Venkataraman, O. Lakkis, A. Madzvamuse [2012] "Global existence for semilinear reaction-diffusion systems on evolving domains,"*J. Math. Biol.*, **64**, pp. 41–67.

J. A. Mackenzie, A. Madzvamuse, [2009] "Analysis of stability and convergence of finite difference method for a reaction-diffusion problem on a one dimensional growing domain." *J. Num. Anal.*, **322(10)**, pp. 891–921.

A. Madzvamuse [2006] " Time-stepping schemes for moving finite elements applied to reaction-diffusion systems on fixed and growing domains." *J. Comp. Phys.* **214**, pp. 239–263.

P. K. Maini, M. R. Myerscough, [1997] " Boundary-driven instability." *J. Appl. Math. Lett* **10(1)**, pp. 1–4.

V. Thomee, L. Wahalbin, [1975] "On Galerkin methods in semilinear parabolic problems." *SIAM J. Num. Anal.* **12(3)**, pp. 378–389.

O. Lakkis, A. Madzvamuse, C. Venkataraman, [2014] "Implicit-explicit timestepping with finite element approximation of reaction-diffusion systems on evolving domains." *SIAM J. Num. Anal.* **51(4)**, pp. 2309–2330.

A. Bonito, I. Kyza, R. Nochetto, [2013] "Time-discrete higher-order ALE formulations: Stability." *SIAM J. Num. Anal.* **51(1)**, pp. 577–604.

A. Madzvamuse, A. H. W. Chung, C. Venkataraman, [2015] "Stability analysis and simulations of bulk-surface reaction-diffusion systems." *Proc. R. Soc. A.* **472(10)**, pp. 891–921.

A. Madzvamuse, E. A. Gaffney, P. K. Maini, [2010] "Stability analysis of non-autonomous reaction-diffusion systems: the effect of growing domains." *J. Math. Biol.* **61**, pp. 133–164.

R. Barreira, C. M. Elliot, A. Madzvamuse, [2011] "The surface finite element method for pattern formation on evolving biological surfaces." *J. Math. Biol.* **63**, pp. 1095–1119.

A. Madzvamuse, H. S. Ndakwo, R. Barreira, [2016] "Stability analysis of reaction-diffusion models on evolving domains: The effect of cross-diffusion." *Discr. Cont. Dyn. Sys.* **36(4)**, pp. 2133–2170.

D. J. Estep, M. G. Lasron, R. D. Williams, [2000] "Estimating the error of numerical solutions of systems of reaction-diffusion equations." *A. Math. Soc.* **146(396)**, DOI: 10.1090/memo/0696.

A. Madzvamuse, P. K. Maini, [2007] "Velocity-induced numerical solutions of reaction-diffusion systems on continuously growing domains." *J. Comp. Phys.* **225**, pp. 100–119.

B. I. Henry, S. L. Wearne, [2007] "Existence of Turing instabilities in a two-species fractional reaction-diffusion system." *J. Comp. Phys.* **62(3)**, pp. 870–887.

A. Gierer, H. Meinhardt, [1972] "A Theory of Biological Pattern Formation." *Springer-Verlag. Berlin,* **12(1)**, pp. 30–39.

T. Erneux, G. Nicolis, [1993] "Propagating waves in discrete bistable reaction-diffusion systems." *Physica. D. North-Holland.* **67**, pp. 237–244.

A. Madzvamuse, P. K. Maini, A. J. Wathen, [2005] "A moving grid finite element method for the simulation of pattern generation by Turing models on growing domains." *J. Sc. Comp.* **24(2)**, DOI: 10.1007/s10915-004-4617-7.

A. Madzvamuse, P. K. Maini, A. J. Wathen, [2003] "A moving grid finite element method applied to a model biological pattern generator." *J. Comp. Phys.* **190**, pp. 478–500.

P. Liu, J. Shi, Y. Wang, X. Feng, [2013] "Bifurcation analysis of reaction-diffusion Schnakenberg model." *Math. Chem.* **51**, pp. 2001-2019.

E. Campillo-Funollet, C. Venkataraman, A. Madzvamuse, [2016] "A Bayesian approach to parameter identification with an application to Turing systems." —- –, DOI:arXiv:1605.04718 [q-bio.QM].

I. Lengyel, I. R. Epstein, [1992] "A chemical approach to designing Turing pattern in reaction-diffusion systems." *Proc. Natl. Acad. Sci. USA.* **89**, pp. 3977–3979.

K. Jin. Lee, W. D. McCormick, J. E. Pearson, [1994] "Experimental observation of self-replicating spots in a reaction-diffusion system." *Nature,* **369**, pp. 215–218.

M. Kim, M. Bertram, M. Pollmann, A. V. Oertzen, A. S. Mikhialov, H. H. Rotermund, [2001] "Controlling chemical turbulance by global delayed feedback: Pattern formation in catalytic CO oxidation on Pt(110)." *Science,* **5520**, pp. 891–921.

N. N. Lebedev, [1965] "Special functions and applications." *SIAM. Review,* **7(4)**, pp. 577-580.

T. Qian, E. Wegert, [2013] "Optimal approximation by blaschke forms." *Complex variables and elliptic equations,* **58(1)**, pp. 122-133, DOI: 10.1137/1007133.

E. Wegert, [2013] "Depicting complex beauty." *Comput. Methods. Funct,* **13(1)**, pp. 3-10.

G. Dimitriu, R. Stefanescu, [2008] "Numerical Experiments for Reaction-Diffusion Equations Using Exponential Integrators." *Int Conf Num Anal App. Springer Berlin Heidelberg* **16**, pp. 249-256.

W. Sarfaraz, A. Madzvamuse, [2017] "Classification of parameter spaces for a reaction-diffusion model on stationary domains." *Chaos, Solitons and Fractals* **103**, pp. 33–51.

Y. Fengji, W. Junjie, S. Junping, [2009] "Bifurcation and spatiotemporal patterns in a homogeneous diffusive predator-prey system." *J. Diff. Eqs* **246**, pp. 1944-1977.

O. Persson, [2015] "Distmesh-a simple mesh generator in matlab." *URL http://persson. berkeley. edu/distmesh/.[Online].*

A. Schnepf, D. Leitner, [2009] "FEM simulation of below ground processes on a 3-dimensional root system geometry using Distmesh and COMSOL Multiphysics." *Proceedings of ALGORITMY* **18**, pp. 321–330.

M. Robert, [2001] "Fundamental theorem of algebra." *Formalized Mathematics* **9(3)**, pp. 461–470.

D. T. Lee, B. J. Schachter, [2001] "Two algorithms for constructing delaunay triangulation." *Int. J. Comp. Inf. Sci* **9(3)**, pp. 219–242.

G. Strang, P. O. Persson, [2004] "A simple mesh generator in MATLAB." *SIAM Review* **46**, pp. 329–345.

J. Schnakenberg, [1979] "Simple chemical reaction systems with limit cycle behaviour." *J. Theor. Biol* **81**, pp. 389–400.

D. Iron, J. Wei, M. Winter, [2003] "Stability analysis of Turing patterns generated by the Schnakenberg model."*Jour. Math. Biol* **49(4)**, pp. 358-390.

C. Xu, J. Wei, [2012] "Hopf bifurcation analysis in a one dimension Schnakneberg reaction-diffusion model."*Nonlin. Anal: Real World Applications* **13(4)**, pp. 1961-1977.

F. Yi, J. Wei, J. Shi, [2009] "Bifurcation and spatiotemporal patterns in a homogeneous diffusive predator-prey system."*J. Diff. Eqs* **265(5)**, pp. 1944-1977.

F. Yi, E. Gaffney, S. Lee, [2017] "The bifurcation analysis of Turing pattern formation induced by delay and diffusion in the Schnakenberg system."*Discr & Cont Dyn Sys-B* **22(2)**, pp. 647-668.

J. D. Murray. [2013] "Mathematical Biology:"*Spatial Models and Biomedical Applications* **5**th. ed, Springer New York.

I. M. Smith, D. V. Griffiths. [1988] "Programming the Finite Element Method. Second Edition:"*Finite Element Method and Data Processing* John Wiley & Sons Ltd. New York.

D. J. Acheson. [1990] "Elementary Fluid Dynamics:"*Oxford Applied Mathematics and Computing Series* Oxford University Press. New York.

M. J. Baines. [1994] "Moving Finite Elements:"*Monographs on Numerical Analysis* Ox. Sc. Pub. UK.

M. G. Larson, F. Bengzon. [2013] "The Finite Element Method:"*Theory, Implementation and Application: Texts in Computational Science and Engineering* Springer. Verlag. Berlin Heidelberg.

W. Huang, R. D. Russell. [2011] "Adaptive Moving Mesh Methods:"*Applied Mathematical Sciences* **174**, Springer. Verlag, New York.

L. E. Keshet. [2005] "Mathematical Models in Biology:"*Classics in Applied Mathematics* Philadelphia. Pa. USA. (SIAM).

L. N. Trefethen. [2000] *Spectral Methods in MATLAB* Philadelphia. Pa. USA. (SIAM), DOI:10.1137/1.9780898719598.

H. E. William. [1931] "Adaptive Moving Mesh Methods:"*The theory of spherical and ellipsoidal harmonics* Cambridge University Press Archive, UK.

A. G. Brown, H. J. Weber. [2001] "Mathematical Methods for Physicists:"*Fifth edition* Harcourt Academic Press, USA.

J. Spanier, K. B. Oldham. [1987] *An Atlas of Functions,* Springer Verlag, Washington, USA.

L. Perko, [1996] "Differential Equations and Dynamical Systems:"*2nd edition* Springer, New York.

C. Venkataraman, [2011] *Reaction-diffusion systems on evolving domains with applications to the theory of biological pattern formation,* Ph.D. thes. Dep. Math, University of Sussex, UK.

A. Madzvamuse, [2000] *A numerical approach to the study of spatial pattern formation,* Ph.D. thes. Math. Inst, University of Oxford, UK.